

## Responses to the reviewer #1:

*This is an interesting and well written paper which discusses the variability of cloud water content, droplet number, and correlation between the two in stratiform clouds. The key findings seem to be the positive correlation between the water content and drop number, and the vertical dependence of this correlation, increasing towards cloud top.*

*The consequences of these results for autoconversion parametrizations is discussed, showing that including the correlation is crucially important for getting the enhancement factor correct, although neglecting variation in drop number entirely is a surprisingly good estimate. I recommend publication after addressing some minor comments I've listed below.*

**Reply:** We thank this reviewer for the encouraging, insightful and constructive comments, which really help improve the manuscript significantly.

Before addressing your comments/questions below, first we would like to provide a summary of the major revisions made to the manuscript:

- We revised significantly the part about the bimodal joint distribution between  $q_c$  and  $N_c$  in section 4. In particular, we pointed out that it is most likely just a coincidence that each side of the “V” shape track sampled one mode of the bimodal distribution. The along/across wind difference between the two sides is unlikely to be the cause of the bimodality.
- Three new cases that are either non-precipitating or weakly precipitating were added to the paper and they have no overall impacts on the conclusions. The flight track and radar reflectivity plots for all the cases, except for July 18, 2017, are provided in the supplementary material.
- A small bug in our code was found and fixed. This bug affects the computation of the EF based on lognormal distributions. As a result, the  $E_q$  based on the lognormal PDF agrees very well with the observation-based  $E_q$  (new Figure 6a), and the  $E$  based on the bivariate lognormal distribution agrees well with the observation-based  $E$  (new Figure 6d). Because of this, the Figure 8 was removed from the paper.
- Most figures are revised/updated per request/suggestion of the reviewers.

After these revisions, we think the paper is much improved and more focused, although the general conclusions still hold.

### *Minor comments*

*1. L45 and elsewhere - does the vertical dependence of EF really need to be accounted for, or would it suffice to simply get it right at cloud top? If the model is correctly representing the domination of accretion throughout the remainder of the cloud (e.g. as in Wood et al (2005b)), then autoconversion and the EF applied to it shouldn't matter so much here.*

**Reply:** Indeed, the autoconversion and accretion have different relative importance at different vertical locations of the cloud. As we pointed out in the paper, most previous studies have ignored the vertical dependence of the EF and the consequential impacts on autoconversion rate simulation. In fact, this is the major motivation of this study. Based on observations, our study reveals that the EF at cloud top is significantly different (smaller) than the lower parts of the

clouds and we also explain the underlying physics. Without a good understanding of the “truth” and underlying physics, how could we make sure that the model “gets it right at cloud top” and also “correctly representing the domination of accretion throughout the remainder of the cloud”?

*2. L103 - it would be worth noting here or later that some CMIP6 models (e.g. Walters et al, 2019, GMD) have adopted variable enhancement factors (better options!) based on the recent work cited, so it's not quite as bad as presented.*

**Reply:** Good point. We revised the paper to point out that the latest generation of GCMs may have adopted more advanced schemes to account for the EF than using a constant EF (around Line 141 in the revised manuscript). On the other hand, it is also important to note that Walters et al (2019) adopted the cloud-regime dependent and scale-aware schemes developed by Hill et al. (2015) and Boutle et al. (2014) to account for subgrid cloud variability. However, even these advanced schemes only consider the subgrid variability of qc only but ignore the variability of Nc and its co-variability with qc. Therefore, they also have important limitations.

*3. L157 - you could also note here that this suggests an equal amount of time should be dedicated to EFs for accretion, something which certainly isn't the case in the literature!*

**Reply:** Good point. We noted here that the vertical dependence is important for both autoconversion and accretion.

*4. L271-273 - are your statistics for variance and correlation then only calculated in regions where  $qc > 0.01 \text{ g/m}^3$ , i.e. over the cloudy portion of the leg which may be  $< 10 \text{ km}$ , or are they calculated over the entire  $> 10 \text{ km}$  leg and include points where  $qc < 0.01 \text{ g/m}^3$  (i.e. the zeros). As this is an important distinction, as it significantly affects the results (as shown in Witte et al, 2019, JAS) and also important for model developers to know to implement correctly in their microphysical parametrization (i.e. does the scheme work on in-cloud quantities or grid-box mean quantities).*

**Reply:** indeed, this is important. All the analyses are based on in-cloud observations (e.g., regions with  $qc > 0.01 \text{ g/m}^3$ ). We pointed this out as suggested.

*5. Section 4.1 - how much do you think the results are affected by the non-stationarity of the cloud being sampled. i.e. for a model parametrization, you are interested in the variability at different heights within the cloud at the same time. But what you are sampling is the variability at different heights in the cloud at different times, up to several hours apart. The cloud is clearly evolving in this time, and how much might that evolution be affecting the results. For example, just looking at the variability in reflectivity in Figure 1 suggests there may be external factors affecting the cloud amount and drop number, and currently this variability is being attributed to the height at which the flight leg during that period happened to be at.*

**Reply:** This is a very good question! It is certainly possible that the selected clouds in this study are “non-stationary”. But it has to be noted that we observed similar vertical variations of qc and Nc in all four selected cases. It seems highly unlikely that the temporal evaluations of the clouds in all four cases conspire to confound our results in the same way. Based on this consideration, we assume that the temporal evolution of clouds is an uncertainty that could lead to random

errors but not the overall conclusions. Of course, it is extremely difficult, if not impossible, to address this issue using air-borne in situ measurements alone due to their inherent limitations as you pointed out. Ground-based radars can provide a reasonable estimate of the vertical profile of  $q_c$  at the temporal-resolution of 5-minutes or so. But currently there is no reliable retrieval of the vertical profile of  $N_c$  from ground radar, yet. The only useful tool in this regard is model simulation. In fact, we are currently simulating the July 18, 2017 case using a LES model which will hopefully help us understand both the spatial and temporal evolution of the clouds and thereby subgrid variability. But this is beyond the scope of this paper. Nevertheless, we pointed out this important limitation at section 4.1 and also at the end of the paper along with other limitations of this study.

*6. Section 4.2 - do you have any hypothesis or theory why  $q_c$  and  $N_c$  are positively correlated? Is there a physical mechanism for the correlation, or just something that happened to be the case for this study? One could imagine that areas with lower  $N_c$  will precipitate easier, thus lowering  $q_c$ ?*

**Reply:** We do think there is some underlying physical processes that could lead to the positive correlation between  $q_c$  and  $N_c$  at cloud top. As you pointed out, one possibility is the autoconversion process itself that converts the cloud water to rainwater and at the same time reducing the  $N_c$ . Another important possibility is the inhomogeneous mixing as a result of cloud top entrainment, which reduces the  $q_c$  and  $N_c$  simultaneously leading to positive correlation between them. We pointed out these possibilities in the revised manuscript.

*7. L491 - as with the comment above, do you think this really is a fortunate cancellation, or is there some underlying physical mechanism?*

**Reply:** As mentioned above, we do believe there is some underlying physical processes that could lead to the positive correlation between  $q_c$  and  $N_c$  at cloud top. As discussed in Eq. (5), because the  $q_c$  and  $N_c$  is positively correlated the  $Ecov$  term is smaller than unity. In contrast, the  $En$  and  $Eq$  terms are always larger than unity. Therefore, it is expected (and explained in the paper) that the  $Ecov$  term tends to cancel the effects of  $En$  and  $Eq$ . But to what extent  $Ecov$  and  $En$  terms cancel out one another depends quantitatively on the variability of  $N_c$  and its correlation with  $q_c$ . But a more important point we would argue is that one should not rely on “fortunate cancellation”. It would be more robust and physically sound to take all three terms, i.e.,  $Eq$ ,  $En$  and  $Ecov$ , into consideration.

*Typos*

*L41 - should say "effect that tends to make".*

*L60 - should probably say "e.g. Morrison and Gettleman" as theirs isn't the first or only scheme out there.*

*L538 - this should say " $Eq$  is significantly larger than  $E$ " I think.*

**Reply:** these typos are all corrected as suggested. Thanks for pointing them out!

## Responses to the reviewer #2:

### General Comments

*This paper uses observational data from the ACE-ENA campaign to assess the horizontal variability and coverability of cloud water content and number concentration. The motivation for this study is the implication of these covariances on the parameterization of autoconversion in coarse resolution models. The study is unique in 2 regards: 1) it focuses on  $q$ - $N$  covariability which is often ignored, and 2) it's evaluation of the coavaribilities as a function of cloud height. The study finds that the so-called enhancement factor for autoconversion decreases robustly from cloud base to cloud top due to increasing correlation between  $q$  and  $N$  at cloud top. These results have important implications for the representation of unresolved cloud microphysical processes in climate and weather models.*

**Reply:** We thank this reviewer for the encouraging, insightful and constructive comments, which really help improve the manuscript significantly.

Before addressing your comments/questions below, first we would like to provide a summary of the major revisions made to the manuscript:

- We revised significantly the part about the bimodal joint distribution between  $q_c$  and  $N_c$  in section 4. In particular, we pointed out that it is most likely just a coincidence that each side of the “V” shape track sampled one mode of the bimodal distribution. The along/across wind difference between the two sides is unlikely to be the cause of the bimodality.
- Three new cases that are either non-precipitating or weakly precipitating were added to the paper and they have no overall impacts on the conclusions. The flight track and radar reflectivity plots for all the cases, except for July 18, 2017, are provided in the supplementary material.
- A small bug in our code was found and fixed. This bug affects the computation of the EF based on lognormal distributions. As a result, the  $E_q$  based on the lognormal PDF agrees very well with the observation-based  $E_q$  (new Figure 6a), and the  $E$  based on the bivariate lognormal distribution agrees well with the observation-based  $E$  (new Figure 6d). Because of this, the Figure 8 was removed from the paper.
- Most figures are revised/updated per request/suggestion of the reviewers.

After these revisions, we think the paper is much improved and more focused, although the general conclusions still hold.

*I only have one critique of this paper. The authors should add non-precipitating clouds to the study. Once the clouds are drizzling the accretion process effectively dominates autoconversion in precipitation production, so in a sense we care more about the autoconversion process (and all of these covariabilities in non-precipitating clouds than we do in the precipitating clouds shown here. Also, there may be important differences between the covariability in non-precipitating and precipitating clouds and it would be informative to understand those differences if they exist.*

**Reply:** Thanks for the suggestion. Indeed, in the original manuscript, we selected only 4 heavily drizzling cases with strong radar reflectivity and precipitation reaching the ground. We didn't select the non-precipitating cloud cases for a couple of reasons. The first reason is to ensure that

autoconversion and accretion processes are active in the selected case. The relevance of an enhancement factor for a cloud not producing precipitation is nebulous. The second reason is more practical. It is because non-precipitating clouds are usually physically thinner than precipitating clouds, which makes it difficult for the airplane to sample different vertical locations of the clouds. As a result, there is often only one or two in-cloud hlegs for the non-precipitating clouds.

Nevertheless, per your suggestion, we selected three non-precipitating or weakly precipitating cases: 1) 2017-07-13 (non-precipitating) 2) 2018-01-26 (weakly precipitating at cloud base but no perception on the ground) 3) 2018-02-07 (very weakly precipitating at cloud base but no perception on the ground) and added them to the revised manuscript. The radar reflectivity curtain with vertical flight track for these three cases are shown in Figure 1 below. The abovementioned challenge of sampling thin non-precipitating cloud can be clearly seen in Figure 1a for the 2017-07-13 case. The selected hlegs and vlegs for these cases are summarized in Table 1. We repeated the same analyses for these new cases as for other cases, i.e., the vertical and horizontal structures of qc and Nc, as well as the EF, for these newly added cases. Overall, the results from these newly added non-precipitating cloud cases are highly similar to those based on the July 18, 2017 case as discussed in section 4. Take the 2018-02-07 case for example. Figure 2 shows the vertical variation of the inverse relative variances  $v_q$  and  $v_N$ . Apparently, both  $v_q$  and  $v_N$  demonstrate a pattern similar to that of the July-18, 2017 case (see Figure 4c of the paper), i.e., increasing first from cloud base (hleg 1  $\rightarrow$  hleg 2) and then decrease toward cloud top (hleg 3). Therefore, these newly added cases do not affect the general conclusion although they add to the statistics.

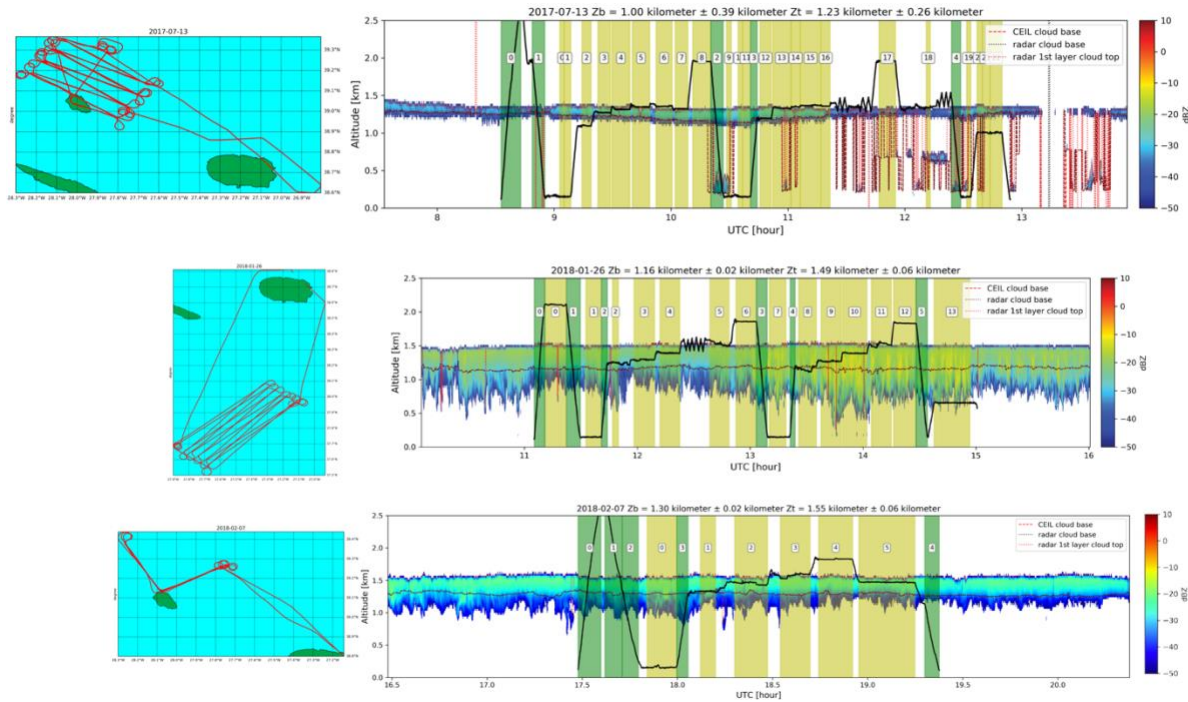


Figure 1 Three non-precipitating (or weakly precipitating) clouds added to the revised manuscript.

*Table 1 A summary of selected RFs, and the selected hlegs and vlegs within each RF. (newly added non-precipitating cases are highlighted in bold font)*

<b>Research Flight</b>	<b>Precipitation</b>	<b>Sampling pattern</b>	<b>Selected hlegs</b>	<b>Selected vlegs</b>
<b>July 13, 2017</b>	<b>Non- Precipitating</b>	<b>Straight-line</b>	<b>3, 4, 5</b>	<b>0, 1, 3</b>
July 18, 2017	Precipitation reaching ground	“V” shape	5, 6, 7, 8, 10, 11, 12	0, 1, 3
Jan. 19, 2018	Precipitation reaching ground	“V” shape	6, 7, 8, 15, 16	0, 1, 3
July 20, 2017	Precipitation reaching ground	“V” shape	5, 6, 7, 8, 9, 13, 14	0, 1
<b>Jan. 26, 2018</b>	<b>Precipitation only at cloud base</b>	<b>Straight-line</b>	<b>3, 4, 5, 9, 10, 11</b>	<b>0, 1, 3</b>
<b>Feb. 07, 2018</b>	<b>Non- Precipitating</b>	<b>“V” shape</b>	<b>1, 2, 3, 5</b>	<b>0, 1</b>
Feb. 11, 2018	Precipitation reaching ground	Straight-line	4, 5, 6, 7, 12, 13	0, 1

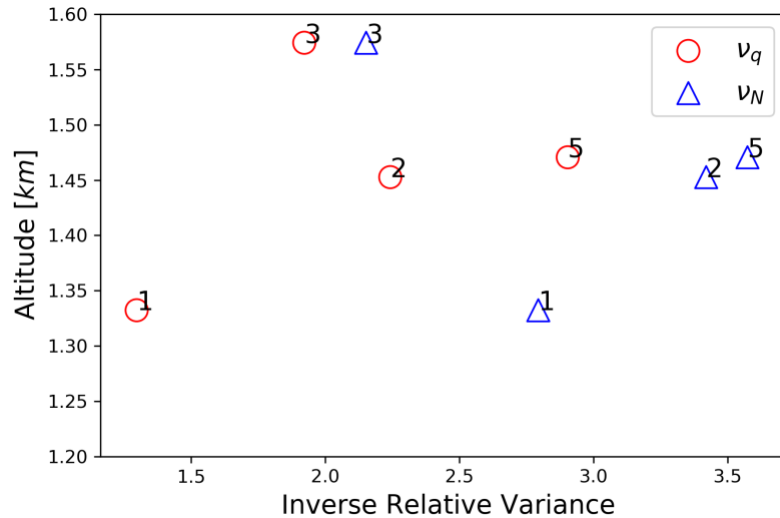


Figure 2 vertical dependence of the inverse relative variances for the Feb. 07 2018 case.

*The paper is very well written, adds to the field, and the methods are sound. I have some editorial comments below and a suggestion for future study. In future studies (not in this paper) I would encourage the authors to look at height dependent correlations between  $q_c$  and  $q_r$  as they relate to accretion. Also understand in the height dependence of the precipitation fraction is critical in representing these unresolved processes.*

**Specific Comments:**

*None*

*Technical corrections:*

*Line 58: process -> processes*

**Reply:** corrected

*Line 370: explain -> explained*

**Reply:** corrected

*Figure 6: Can you put descriptive titles on each subplot or refer to the physical assumptions that correspond to each subplot in addition to referencing the equations to make it easier to figure out what everything means.*

**Reply:** Good suggestion. We added titles to each subplot of Figure 6 and some other figures.

*Line 485 abroad -> broad*

**Reply:** corrected

*Lines 537:  $E_q$  is used twice to mean two different things.*

**Reply:** The second  $E_q$  should be  $E$



### Responses to the reviewer #3

#### *Overview:*

*In addition to being interesting, I think this study is well thought out and the manuscript is well written. I found reading it to be a pleasure. In particular, I would like to compliment the authors on the quality of the introduction. That said, I do have one major concern (general comment #1, below) and several suggestions that might improve the manuscript.*

#### *Recommendation: Publish after major revisions*

*I have labeled this as a major revision, out of concern that responding to general comment #1 may require regenerating most of the figures in the manuscript and I want to give the authors ample time to do this, if necessary. This should not be taken to mean this is a poor work. I think it is excellent.*

**Reply:** We thank this reviewer for the encouraging, insightful and constructive comments, which really help improve the manuscript significantly.

Before addressing your comments/questions below, first we would like to provide a summary of the major revisions made to the manuscript:

- We revised significantly the part about the bimodal joint distribution between  $q_c$  and  $N_c$  in section 4. In particular, we pointed out that it is most likely just a coincidence that each side of the “V” shape track sampled one mode of the bimodal distribution. The along/across wind difference between the two sides is unlikely to be the cause of the bimodality.
- Three new cases that are either non-precipitating or weakly precipitating were added to the paper and they have no overall impacts on the conclusions. The flight track and radar reflectivity plots for all the cases, except for July 18, 2017, are provided in the supplementary material.
- A small bug in our code was found and fixed. This bug affects the computation of the EF based on lognormal distributions. As a result, the  $E_q$  based on the lognormal PDF agrees very well with the observation-based  $E_q$  (new Figure 6a), and the  $E$  based on the bivariate lognormal distribution agrees well with the observation-based  $E$  (new Figure 6d). Because of this, the Figure 8 was removed from the paper.
- Most figures are revised/updated per request/suggestion of the reviewers.

After these revisions, we think the paper is much improved and more focused, although the general conclusions still hold.

#### *General Comments:*

##### *1) Bimodality in the relationship between $q_c$ and $N$*

*My only major concern with the analysis is that the bimodality in the relationship between  $q_c$  and  $N_c$  has a significant impact on the results. The manuscript documents that this bimodality is associated with systematically different values for  $N$  measured when the aircraft was flying either along and across the wind. It seems to me that it is extremely unlikely that this would happen by random chance (that the aircraft just happened to observe a cloud field with two distinction regions with differing  $N$  that happen to align with the flight tracks) given that the same offset is found between legs occurring at different times and different altitudes. I can't think*

*of any physical reason why this should occur. As such it seems to me that it is very likely that this is a measurement artifact. Accordingly:*

**Reply:** Indeed, this is a very interesting and puzzling phenomenon/observation. Although we believe the bimodality is “real” (in other words, it is unlikely an instrument artifact), we think it is most likely just a coincidence that each mode is sampled by one side of the “V” shape track. We do NOT think that the difference in wind pattern (i.e., along wind vs. across wind) “causes” bimodality. Instead, the two sides of the “v”-shaped happen to sample different regions of the “virtual” grid box that have different qc-Nc relations. One can imagine that, if the airplane can sample every point in the “virtual” grid box, then there would be no along-wind vs. across-wind (or from a different perspective, all points can be either along wind or across wind). So, there is no causal relation between along/across-wind difference and the bimodality. They are both results of “v”-shaped sampling pattern. On the other hand, it is important to note that a bimodal sub-grid joint PDF between qc and Nc can very well exist in the nature, which could be a result of sub-grid variation of, for example, vertical draft velocity, precipitation and/or CCN.

In short, we argue that the bimodal joint PDF of qc and Nc is “real”, but it is not a result of the along/across wind pattern difference. We will further elaborate on this point in the context of your questions/comments. We have also revised the manuscript accordingly.

*(A) Discussion: Is it real?*

*Am I missing something simple? In general, I think the possible causes of this systematic shift need to be discussed.*

**Reply:** As we explained above, we do believe that the observed bimodal joint PDF between qc and Nc is “real”. Perhaps, we should not have emphasized the along-wind vs. across wind difference between the two sides of the v shape flight, as it is most likely just a coincidence.

In the revised the manuscript, we point it out that the along/across wind difference and the bimodal joint PDF are likely coincidence. We also pointed it out that some sub-grid variations, for example, vertical draft velocity, precipitation and/or CCN can lead to bimodal joint PDF between qc and Nc.

*(B) Subdivide the horizontal leg data between along and cross wind directions. All of the analysis is based on analyzing full length of the horizontal legs, which if I understand correctly mean the outer scale is about 60 km. That is, the enhancement factors you present represent the enhancement in going from the ~10 m scale of the FCDP measurement to a nominal grid scale of ~60 km. This is a choice you made. There is (as far as I can see) nothing that prevents you from dividing your hlegs into separate along and cross wind legs (I presume each will be about 30 km) and instead examine the variability on this smaller scale ~30 km scale. Obviously doing this will increase the sampling uncertainty associated with each leg, but you will have twice the number of points in most of your figures and more critically it will significantly reduce the impact of any measurement bias in N associated with the along or cross wind measurements.*

**Reply:** Yes, your understanding is correct. We are using the high-resolution (~10 m) FCDP measurements to investigate the sub-grid scale variations of qc and Nc for a nominal GCM grid of 60 km. We made the choice *not* to separate the two sides of the “v” shape flight because the

current generation GCMs usually have a typical resolution of ~100km. A ~60 km grid box would be more relevant to climate modeling in this regard.

Before we submitted the manuscript, we had already done the sensitivity study as your suggested, i.e., separating the two sides of “v” shape flight for the July 18, 2017 case. The new hlegs after the resampling are shown in Figure 1 below. We selected the new hlegs #6 to #13 (corresponding to the original hleg #5 to #8) and #16 to #21 (corresponding to the original hleg #10 to #12) for further analysis. As listed in Table 1, the new hlegs 6, 9, 10, 13, 16, 19, 20 are from the west side of the “v” shape flight (along-wind) and 7, 8, 11, 12, 17, 18, 21 are from the east side of the “v” shape flight (across-wind)

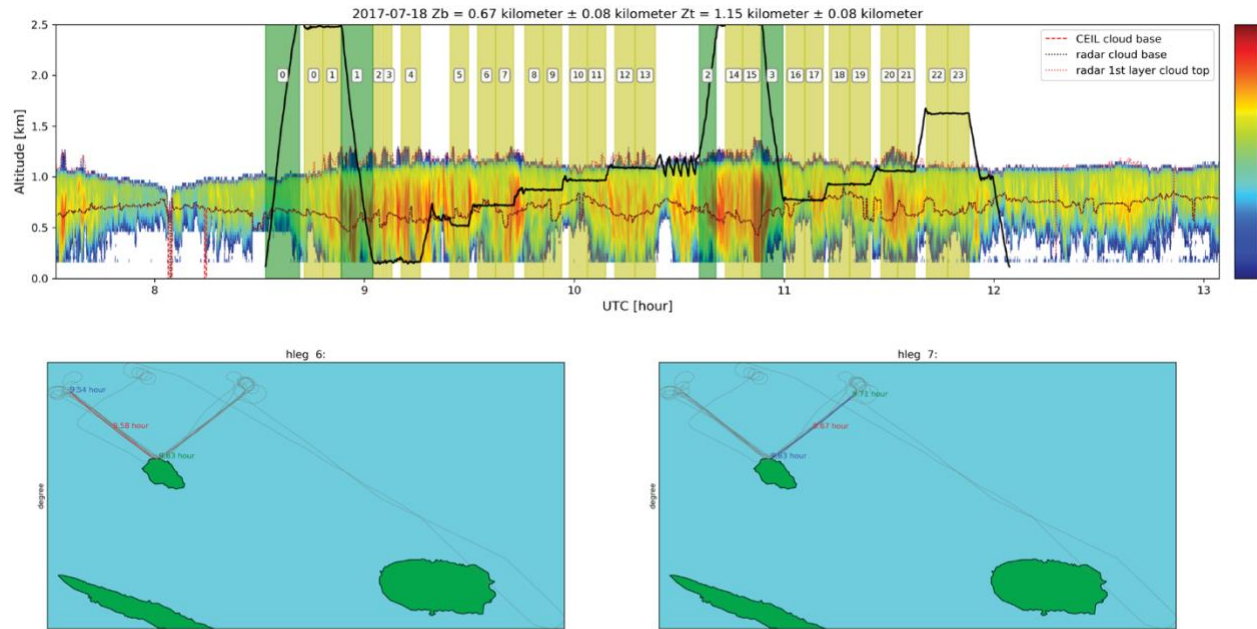


Figure 1 re-sampling of the hlegs for the July 18, 2017 case. Upper panel: The vertical flight track plotted on radar reflectivity measurements. Lower panel: an example to show that after the resampling, the new hleg #6 and #7 each corresponds one side of the “v” shape flight.

Table 1 The selected hlegs after the resampling

	West side of “v” shape (along wind)	East side of “v” shape (across wind)
New hlegs	6, 9, 10, 13, 16, 19, 20	7, 8, 11, 12, 17, 18, 21

After the resampling, the first thing we checked is whether the two modes of the bimodal joint PDF actually correspond to the two sides of the “v” shape flight. And indeed, it is the case.

Then, we repeated the same analysis as we did in Figure 4 and 6 of the original paper for the new hlegs, now with the two sides of the “v” shape flight separated. The key results are summarized in Figure 2. Evidently, both the west side hlegs (Figure 2 a-c) and east side hlegs (Figure 2 d-f)

demonstrate the same vertical structures which are also consistent with those shown in Figure 4 and 6 of the paper: 1) the inverse relative variances  $v_q$  and  $v_N$  first increases from cloud base to cloud top and then decreases. 2)  $q_c$  and  $N_c$  become increasingly correlated from cloud base to cloud top. And 3) the total EF decreases from cloud base to cloud top.

These results clearly demonstrate that our conclusions are robust regardless whether or not we separate the “v” shape flight into two sides. We would like to hold onto the original results and plots based on the whole “v” shape flight in the manuscript for two reasons: 1) ~60 km spatial scale is more relevant to the current GCMs and 2) the bimodal joint PDF is possible and its implications for EF and thereby warm rain simulation should be discussed.

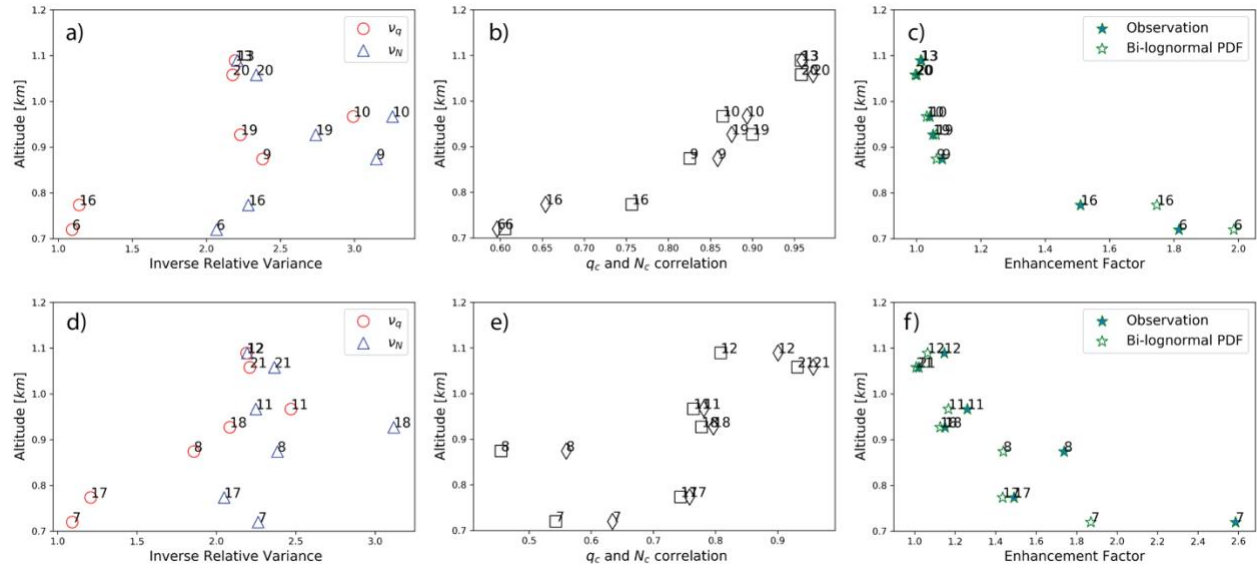


Figure 2 a) vertical variations of a)  $v_q$  and  $v_N$  b)  $q_c$  and  $N_c$  correlation, and c) the total EF for the new hlegs 6, 9, 10, 13, 16, 19, 20 (west side of the “v” shape flight); d) e) and f) are same as a), b) c), respectively, except or for the new hlegs 7, 8, 11, 12, 17, 18, 21 (east side of the “v” shape flight).

## 2) Flying in and out of cloud?

*How are data for those legs where the aircraft goes in and out of cloud being handled? I assume that you didn't include a lot of zeros in either  $q_c$  and/or  $N$  when calculating the means and variances, or for that matter, the directly calculating  $E$  values (e.g., equation 9)? Please describe what was done and comment on the impact this might have on the results.*

**Reply:** As explained in the section 4.1, we use  $q_c > 0.01 \text{ gm}^{-3}$  as the threshold to mask cloudy against clear-sky observations. All of our analyses are based on in-cloud measurements. In other words, we exclude zero values in the computations of  $v_q$ ,  $v_N$ ,  $E_q$ ,  $E_N$  or  $E$ , etc. For example, the  $P(q_c)$  in Eq. (6) is the in-cloud PDF of  $q_c$  in a GCM grid. We have explicitly point this out at the beginning of Section 4.1. In addition, to avoid potential confusion, we have replaced the lower limit of the integration in Eq. 3, 9 and 10 from zero to minimal in-cloud values  $q_{c,min}$  and  $N_{c,min}$ .

## 3) Inner Scale Dependence

*One of the most interesting points in the paper is that the PDF of  $N$  is not lognormally distributed near the boundaries. It seems to me that this is likely due to entrainment*

*preferentially evaporating the smallest cloud droplets first. The time series is very spikey in nature (spikes having low  $N$  values). This suggests to me that this effect might be greatly reduced if you started from a larger inner scale (100 or 200 m) rather than the  $\sim 10$  m.*

*I think it would be a nice addition to your analysis to first average the FCDP data to a scale of 100 to 200 m (use 1 Hz data) and examine how this impacts the skewness of the distributions and the ability of the bivariate log normal to model the variability and enhancement factors.*

**Reply:** Following your suggestion, we did a sensitivity study using 1 Hz FCDP data (instead of the original 10 Hz) for the analysis. As an illustrative example, Figure 3 shows  $q_c$  and  $N_c$  time series based on 1 Hz (upper panel) vs. 10 Hz (lower panel) FCDP observations for the hleg #8 at cloud top.

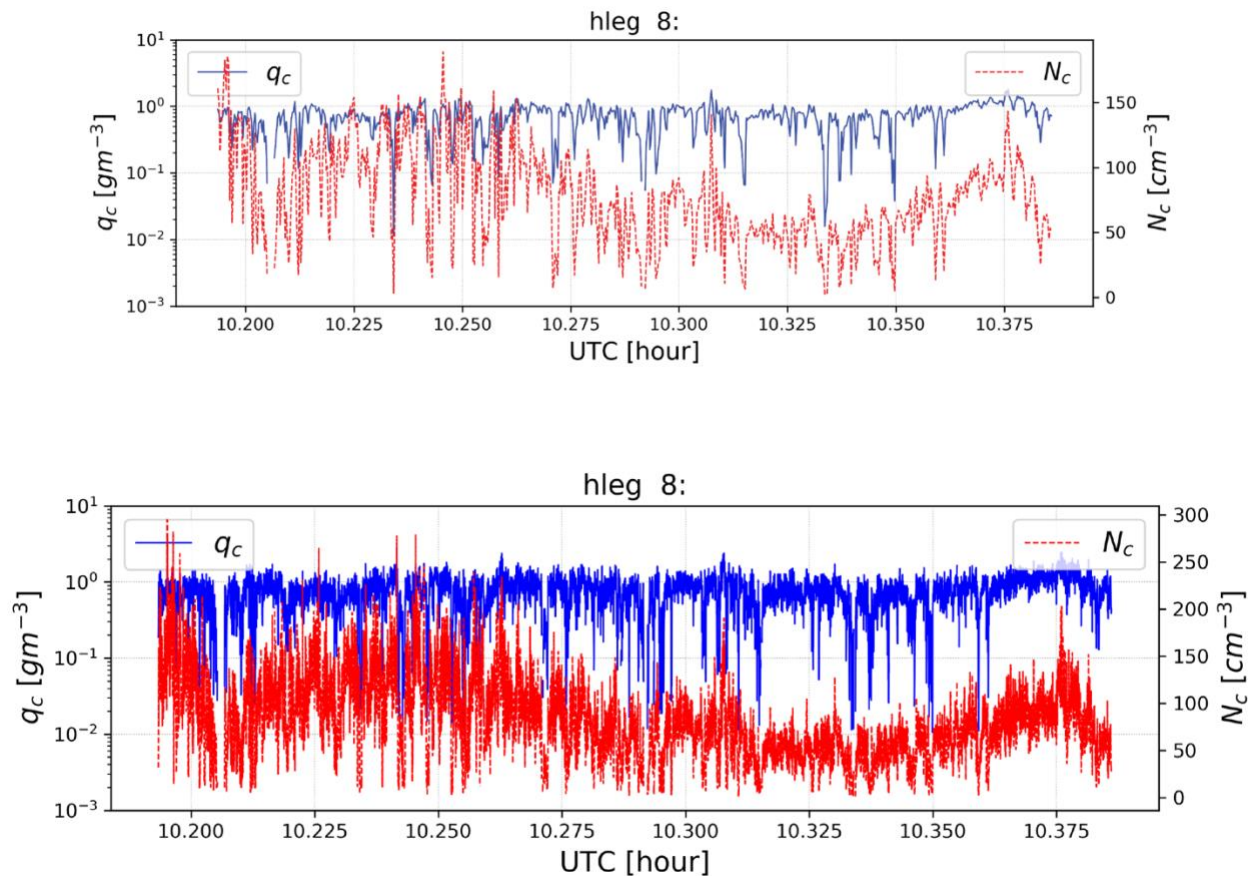


Figure 3  $q_c$  and  $N_c$  time series based on 1 Hz (upper panel) vs. 10 Hz (lower panel) FCDP observations.

Using the 1 Hz data, we repeated all the analyses we did for the July 18, 2017 case. As shown in Figure 4 and Figure 5, the results are almost identical to those based on 10 Hz data. Therefore, we can conclusions hold for both 10 Hz and 1 Hz FCDP data.

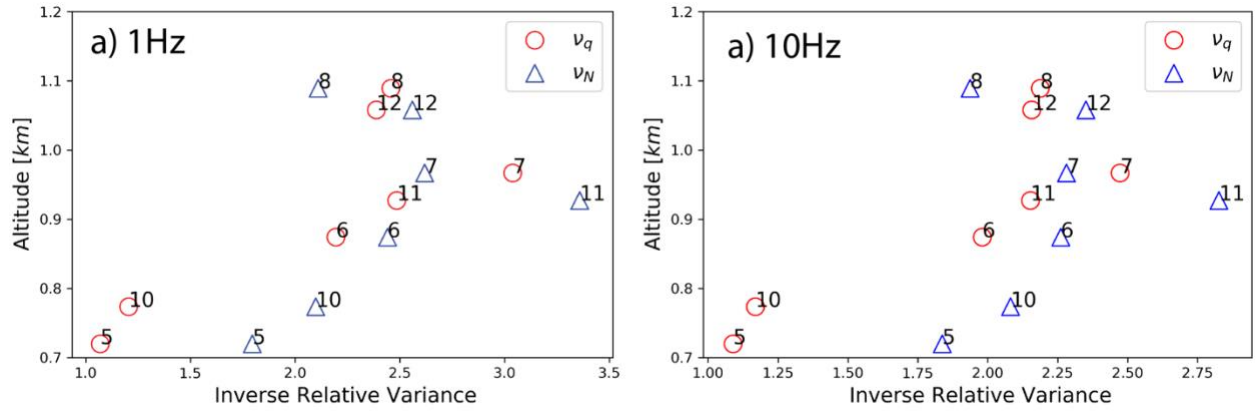


Figure 4 inverse relative variances based on a) 1Hz and b) 10Hz

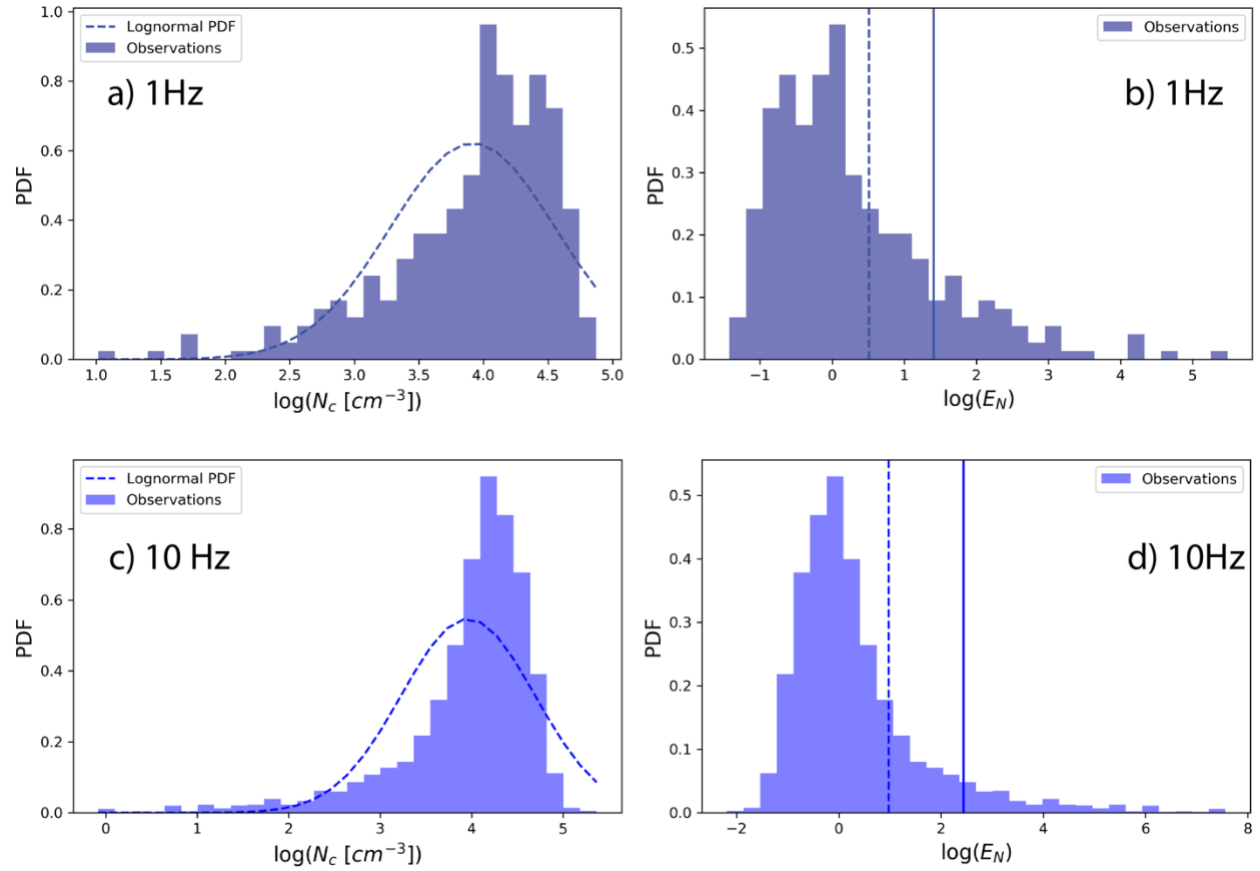


Figure 5 Analysis of the  $E_N$  bias for hleg 10 based on 1 Hz FCDP data (a and b) vs. 10 Hz FCDP data (c and d).

#### 4) Dependency rather than trend

*I think the discussion is overly focused on whether there is a (linear) trend in the data. Let's look at Figure 9. To me, "trend" just doesn't seem like the right word to describe the situation in Figure 9a. I suggest a more apt description might be, "Figure 9a shows significant scatter in  $E$  with altitude, with smaller values and relatively little scatter near cloud top, and decidedly larger values near cloud base."*

*I understand entirely that the change with height projects on to a line and the correlation is significant. There is a vertical dependence. But it is not obvious to me that there is a linear dependence or trend.*

*Importantly I see Figure 9c has this same pattern, with larger  $En$  values (on average) at the bottom than the top, as does 9b for  $E_q$  with the exception of the two outliers near cloud top.*

*Somewhat similarly in 9d, the correlations are clearly stronger and there is less variability near cloud top. But it is not clear to me there is a linear dependence. I note the bimodal points are causing much of the variability mid-cloud.*

*I recognize this is partly philosophical, but I think it would be better to recast some of the discussion in terms of a there being a vertical dependence rather than a “trend”, though perhaps with more points (general comment 1b) a trend will become clearer.*

**Reply:** Good point! We put all the cases together in Figure 9 in hoping to see if there is any common feature. And the only common features we could observe are the decreasing “trends” in  $E$  (Figure 9 a) and increasing “trend” in  $\rho$  (Figure 9d). But we agree with your observation that it is not very convincing to call it a trend. Indeed, the vertical variation of  $v_q$ ,  $v_N$ , and thereby EF are unlikely going to be linear. On the other hand, because of the limited sampling rate and the big differences among the selected cases, it is hard, if not impossible, to resolve both horizontal and at the same time the detailed vertical variations of cloud properties using the in situ measurements. We revised the manuscript following your suggestions and also pointed out the caveats when interpreting the results in Figure 6 and 9 (at the end of Section 4.1).

*Specific Comments:*

*Line 213. What is the WCM-2000? Please provide a reference and perhaps add to table #1. Perhaps add a figure demonstrating agreement in qc, or at least quantify what “excellent” agreement means (e.g. Bias less than X and RMS difference less than Y% at 10 Hz?). I note here that this study is about variability and so ideally it would be good to establish variability in qc is the same from both sensor (not simply that the bias between two measurements is small).*

**Reply:** WCM stands for “Water Content Measurement” (“2000” is just a model number). We added a reference (Alyssa and Mei) for this instrument. We compared the qc from FCDP with the WCM measurements for the selected hlegs of the July 18, 2017 case. The mean values of the two measurements are generally within 20% (this information is added to the manuscript as suggested). We have consulted the DOE measurement team (i.e., Fan Mei) and confirmed that the difference is reasonable. The two instruments seem to have a time lag, probably due to the instrument response difference. The instrument differences are beyond the scope of this study.

*Table #1. Perhaps change label “Accuracy” to “Particle Size Intervals” or something similar?*

**Reply:** Good suggestion. We changed to “size resolution”.

*Line 214. A value of 20 microns for  $\gamma_{IS}^*$  is about as small a threshold as might be chosen, and there are often a significant number of particles in the 20 to 50 micron size range for clouds that are described as “non precipitating”. I expect particle concentrations in the 20 to 50 micron size range will co-vary with the concentration of particles less than 20, so I am not surprised that you see little sensitivity. Nonetheless I think it would have been better test of the sensitivity by*

choosing values for  $r^*$  of 20 and 50, rather than  $20 \pm 5$ . In particular, you show later in the manuscript that  $N$  (with the cut off of  $r^*$  of 20) is not well described by a lognormal near cloud-top or cloud-base. Is this result sensitive to the choice of  $r^*$ ?

**Reply:** The  $r^*$  is the threshold used to separate the “cloud mode” and “precipitation mode”, and also the autoconversion and accretion processes. As explained in the paper, we choose  $r^*=20 \mu\text{m}$  to follow previous studies (e.g., Wood 2005).  $r^*=50 \mu\text{m}$  seems too large too us. Nevertheless, we did a sensitivity study in which we set  $r^*=50 \mu\text{m}$  and got almost identical results (see Figure 6 below). Your expectation is correct. The results are not sensitive to the choice of  $r^*$ .

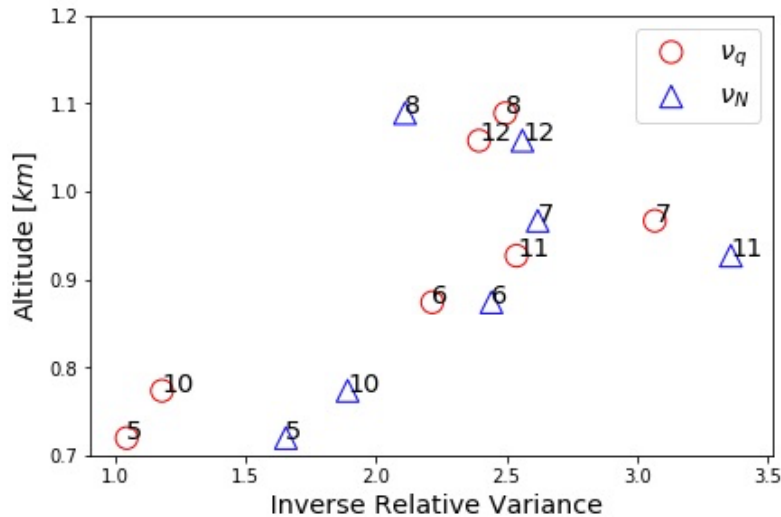


Figure 6 Inverse relative variance plot when set  $r^*=50 \mu\text{m}$

Line 238. Do I understand correctly that only flight labeled as drizzling in table #2 were considered? If so, how were the groupings in Table #2 established? Does “non precipitating” in table #2 mean only particles less than 20 microns where present OR Only when drizzle is clearly falling from clouds (from radar and “pilots” on line 269)?

Perhaps it doesn't matter for this paper, but I presume models will apply autoconversion rate parameterizations all the time and I think it would be useful to examine precipitation formation for cloud without obvious precipitation / virga falling from the bottom OR otherwise clearly establish the conditions under which your results apply.

**Reply:** Reviewer #2 raised somewhat similar questions. At the beginning, we used the pilot summary in table #2 to narrow down our search for heavily drizzling cases. Then, we manually selected the 4 cases mainly based on radar observations (i.e., strong radar reflectivity with precipitation reaching surface). We didn't select the non-precipitating cloud cases for a couple of reasons. The first reason is that we would like to make sure that the drizzling processes, including both autoconversion and accretion have been initialized in the selected case. The second reason is more practical. It is because non-precipitating clouds are usually physically thinner than precipitating clouds, which makes it difficult for the airplane to sample different vertical locations of the clouds. As a result, there is often only one or two in-cloud hlegs for the non-precipitating clouds.

Nevertheless, per your suggestion, we selected three non-precipitating or weakly precipitating cases: 1) 2017-07-13 (non-precipitating) 2) 2018-01-26 (weakly precipitating at cloud base but no perception on the ground) 3) 2018-02-07 (very weakly precipitating at cloud base but no perception on the ground) and added them to the revised manuscript. The radar reflectivity curtain with vertical flight track for these three cases are shown in Figure 7 below. The abovementioned challenge of sampling thin non-precipitating cloud can be clearly seen in Figure 1a for the 2017-07-13 case. The selected hlegs and vlegs for these cases are summarized in Table 2. We repeated the same analyses for these new cases as for other cases, i.e., the vertical and horizontal structures of qc and Nc, as well as the EF, for these newly added cases. Overall, the results from these newly added non-precipitating cloud cases are highly similar to those based on the July 18, 2017 case as discussed in section 4. Take the 2018-02-07 case for example. Figure 8 shows the vertical variation of the inverse relative variances  $\nu_q$  and  $\nu_N$ . Apparently, both  $\nu_q$  and  $\nu_N$  demonstrate a pattern similar to that of the July-18, 2017 case (see Figure 4c of the paper), i.e., increasing first from cloud base (hleg 1  $\rightarrow$  hleg 2) and then decrease toward cloud top (hleg 3). Therefore, these newly added cases do not affect the general conclusion although they add to the statistics.

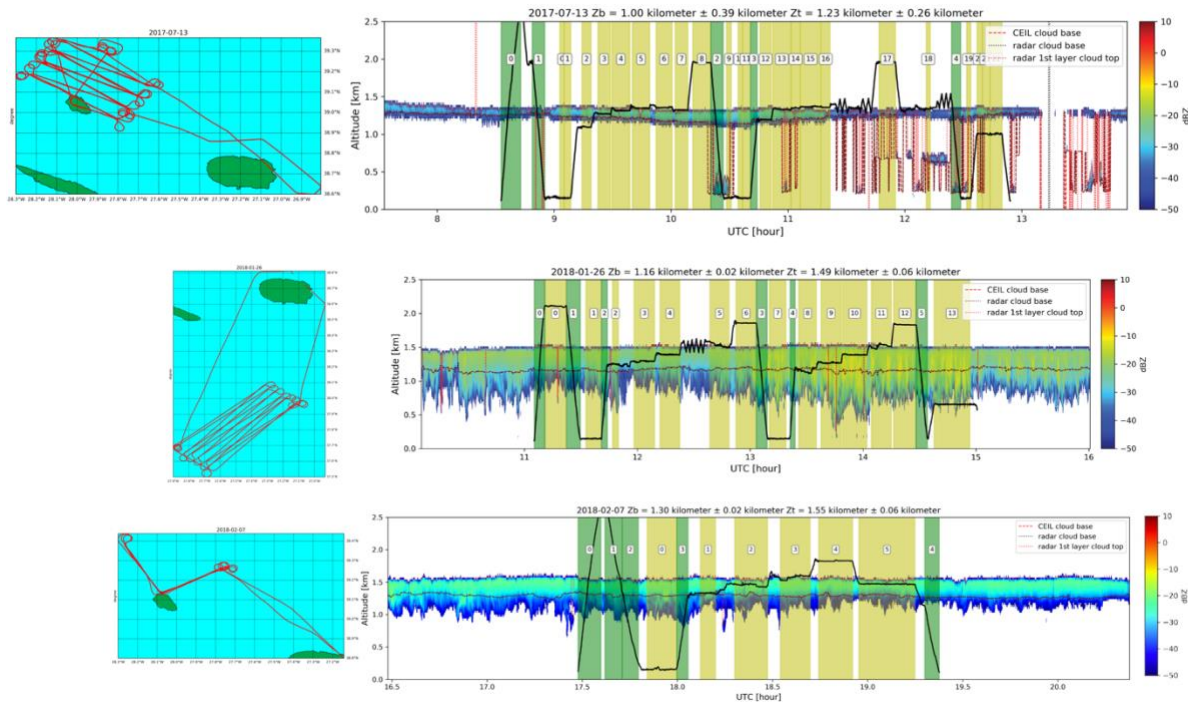


Figure 7 Three non-precipitating (or weakly precipitating) clouds added to the revised manuscript.

Table 2 A summary of selected RFs, and the selected hlegs and vlegs within each RF. (newly added non-precipitating cases are highlighted in bold font)

Research Flight	Precipitation	Sampling pattern	Selected hlegs	Selected vlegs

<b>July 13, 2017</b>	<b>Non- Precipitating</b>	<b>Straight-line</b>	<b>3, 4, 5,</b>	<b>0, 1, 3</b>
July 18, 2017	Precipitation reaching ground	“V” shape	5, 6, 7, 8, 10, 11, 12	0, 1, 3
Jan. 19, 2018	Precipitation reaching ground	“V” shape	6, 7, 8, 15, 16	0, 1, 3
July 20, 2017	Precipitation reaching ground	“V” shape	5, 6, 7, 8, 9, 13, 14	0, 1
<b>Jan. 26, 2018</b>	<b>Precipitation only at cloud base</b>	<b>Straight-line</b>	<b>3, 4, 5, 9, 10, 11</b>	<b>0, 1, 3</b>
<b>Feb. 07, 2018</b>	<b>Non- Precipitating</b>	<b>“V” shape</b>	<b>1, 2, 3, 5</b>	<b>0, 1</b>
Feb. 11, 2018	Precipitation reaching ground	Straight-line	4, 5, 6, 7, 12, 13	0, 1

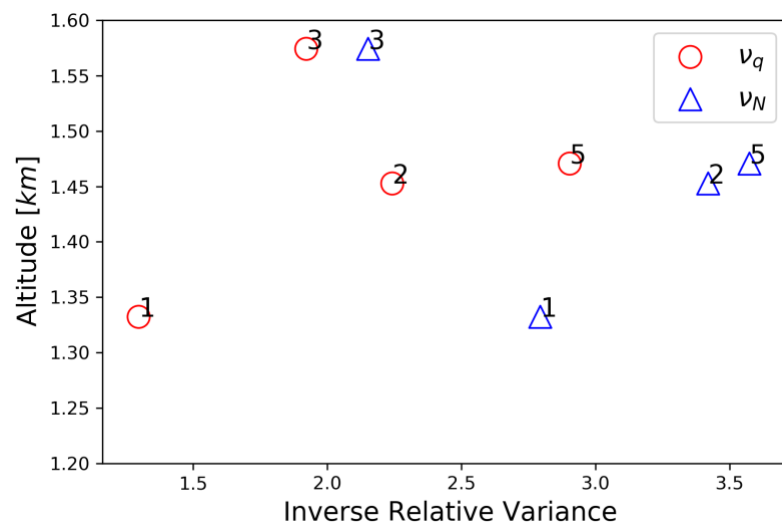


Figure 8 vertical dependence of the inverse relative variances for the Feb. 07 2018 case.

Line 269. I don't fully understand this criteria or how it is being applied. Is this requirement applied to each horizontal leg or just for choosing cases (see comment for line 238)? If individual legs, are you focusing on the portion of the leg that occurs near the

*radar? Is there a reflectivity threshold? In general, you have CDP and 2DS data and so I don't understand the choice to rely on radar or pilots.*

**Reply:** Since we added the non-precipitating cloud cases, this criterion is removed. For your information, the criterion was originally applied to research flights in table #2 rather than hlegs.

*Line 274. Does “same region” here mean the hlegs must occur along roughly the same track, that is the same set of latitudes and longitudes? If yes, I don't understand the rationale for this. As long as you are sampling the same cloud field (i.e. it is reasonable to expect a representative measure of the variability) and you are using hlegs with the same total length, why do you care if the hlegs are nominally stacked?*

**Reply:** By “same region” we mean that the selected hlegs should be within the same “virtual” GCM grid box. The hlegs do not have to be “nominally stacked”. Take the July 18, 2017 case for example. All the “v”-shape legs naturally formed a “virtual” grid-box. Although the airplane repeated many “v”-shape legs, there are also long transient flights (See Figure 1a of the paper). We excluded these flights because they are outside of the “virtual” grid-box.

*Line 332. Previous studies? Please provide a reference.*

**Reply:** The following references are added: Barker 1996, Lebsock et al. 2013 and Zhang et al. 2019.

*Line 443. “slight”? It is not clear to me whether this difference would or would not have a significant impact on a model simulation. Perhaps just indicate the bivariate lognormal results in an EF value that is about 0.5 larger (be quantitative rather than qualitative).*

**Reply:** Thanks for raising this question. Actually, after examination we found a small bug in our codes (see explanation at the beginning). The Eq based on lognormal parameterization are actually very close to observation-based values, which is consistent with our previous finding in Zhang et al. 2019. The mean bias is only 0.06. this result. This information is added to the revised paper.

*Line 541. It seems natural to expect qc and N will be positively correlated, since stronger updraft mean both activating more droplets and condensing more water.*

**Reply:** Yes, this is one possible reason. Another possibility is the inhomogeneous mixing due to cloud top entrainment, which reduces the qc and Nc simultaneously. In this study, we can only speculate about the possible reasons. At the moment, we are also using LES to investigate the underlying physics.

*Line 503-12. The use of a “relative hleg altitude” seem to me to be “just as prone” or even “more prone” to misinterpretation as using cloud boundaries from either radar/lidar or the vlegs. Here you are effectively demanding that the highest and lowest legs in each flight should have the same relationship regardless of how close or far they are from the actual cloud top or cloud base. I guess the question is, does it matter? Based on your 4th criteria (line 281) I would hope not.*

**Reply:** As one can see from Figure 1 of the paper, the selected cases are quite different in terms of cloud thickness and cloud boundaries. So, to make any meaningful comparison, we have to first normalize the boundary of each case, which lead us to the use of “relative hleg altitude”.

We can the cloud boundaries either from in-situ or radar/lidar measurements for the normalization, although uncertainties are inevitable either way.

Due the field campaign, the pilot was actually instructed to sample the cloud base and cloud top as close as possible because these observations are very useful for studying clouds (e.g., understanding cloud top entrainment and cloud base precipitation). However, it is still extremely difficult to determine cloud boundaries from in situ measurements alone. This is why we have required that the in situ and radar/lidar measurements are largely consistent (i.e., the *4th criteria* (line 281)”)

*Minor Comments*

*Line 55-6. Replace “. . . at the spatial scales much smaller .. ” with “. . . on spatial scales that are much smaller . . .”*

**Reply:** Done

*Line 56-7. Remove the phrase “. . . making the simulation of these processes in GCMs highly challenging.” This is entirely redundant with the “challenging” remark on the previous sentence.*

**Reply:** Done

*Line 164. Perhaps rephrase as “. . . better understand the horizontal variations in*

**Reply:** ok done.

*Line 184. Replace “seasonable” with “seasonal”*

**Reply:** Done.

*Line 185. Perhaps add comma and remove “and” so the sentence reads “. . . the MBL (Dong et al., 2014; Rémillard 185 et al., 2012), to improving cloud parameterizations in the GCMs (Zheng et al., 2016), to validating the space-borne remote sensing products of MBL clouds (Zhang et al., 2017).”*

**Reply:** Good suggestion. Done.

*Line 189. Change “is” to “was”, and perhaps simplify to read “In 2013 a permanent measurement site was established by the ARM program on Graciosa Island, and is typically referred to as the ENA site (Voyles and Mather, 2013).”*

**Reply:** Done.

*Figure 1. I presume the green blobs are islands? Perhaps explain this in the caption along with note about location of the ARM site and likewise describe what the number in white boxes and colored stripes mean in radar panels? Also I suggest higher resolution figure would be helpful here.*

**Reply:** Yes, they are islands. Figure 1 has been revised following your suggestions and figure captions updated. Note that we have moved the figures for other selected cases to the supplementary materials so we can use high-resolution and larger figures for July 18, 2017 case.

*Figure 9. The solid symbols seem a bit problematic here. I am pretty sure that in panel c, there is a red dot near cloud top that must be hidden under the other symbols – and this make me wonder if other symbols might also be hidden.*

**Reply:** we revised the figure using open symbols to reduce overlap.

*Line 537. I think you mean “ $E_q$  is larger than  $E$ ”, and you need to change the second occurrence of  $E_q$  in this sentence to be simply  $E$ .*

**Reply:** yes, you are right. We corrected this.

*Line 561. Perhaps change to read “... implications of subgrid variability as relates to the enhancement of autoconversion rates ...”*

**Reply:** Thanks for the suggestion. We revised accordingly.

*Line 566. Perhaps add “near cloud top” to the end of the sentence. I think it is reasonable to make the association with cloud-top entrainment but obviously, the study doesn’t define entrainment zone as best I recall.*

**Reply:** Changed to “near cloud top”.

*Line 569. Change “we” to “our”.*

**Reply:** Done.

**Vertical Dependence of Horizontal Variation of Cloud Microphysics:  
Observations from the ACE-ENA field campaign and implications for warm rain  
simulation in climate models**

Zhibo Zhang<sup>1,2,\*</sup>, Qianqian Song<sup>1,2</sup>, David B. Mechem<sup>3</sup>, Vincent E. Larson<sup>4</sup>, Jian Wang<sup>5</sup>,  
Yangang Liu<sup>6</sup>, Mikael K. Witte<sup>7,8</sup>, Xiquan Dong<sup>9</sup>, Peng Wu<sup>9,10</sup>

1. Physics Department, University of Maryland Baltimore County (UMBC), Baltimore,  
21250, USA

2. Joint Center for Earth Systems Technology, UMBC, Baltimore, 21250, USA

3. Department of Geography and Atmospheric Science, University of Kansas, Lawrence,  
66045, USA

4. Department of Mathematical Sciences, University of Wisconsin — Milwaukee,  
Milwaukee, 53201, USA

5. Center for Aerosol Science and Engineering, Department of Energy, Environmental and  
Chemical Engineering, Washington University in St. Louis, St. Louis, 63130, USA

6. Environmental and Climate Science Department, Brookhaven National Laboratory,  
Upton, 11973, USA

7. Joint Institute for Regional Earth System Science and Engineering, University of  
California Los Angeles, Los Angeles, 90095, USA

8. Jet Propulsion Laboratory, California Institute of Technology, Pasadena, 91011, USA

9. Department of Hydrology and Atmospheric Sciences, University of Arizona, Tucson,  
85721, USA

10. Pacific Northwest National Laboratory, Richland, WA 99354, USA

To be submitted to the ACP special issue: Marine aerosols, trace gases, and clouds over the  
North Atlantic

*Correspondence to:* Zhibo Zhang (zhibo.zhang@umbc.edu)

## Abstract:

In the current global climate models (GCM), the nonlinearity effect of subgrid cloud variations on the parameterization of warm rain process, e.g., the autoconversion rate, is often treated by multiplying the resolved-scale warm rain process rates by a so-called enhancement factor (EF). In this study, we investigate the subgrid-scale horizontal variations and covariation of cloud water content ( $q_c$ ) and cloud droplet number concentration ( $N_c$ ) in marine boundary layer (MBL) clouds based on the in-situ measurements from a recent field campaign, and study the implications for the autoconversion rate EF in GCMs. Based on a few carefully selected cases from the field campaign, we found that in contrast to the enhancing effect of  $q_c$  and  $N_c$  variations that tends to make  $EF > 1$ , the strong positive correlation between  $q_c$  and  $N_c$  results in a suppressing effect that tends to make  $EF < 1$ . This effect is especially strong at cloud top where the  $q_c$  and  $N_c$  correlation can be as high as 0.95. We also found that the physically complete EF that accounts for the covariation of  $q_c$  and  $N_c$  is significantly smaller than its counterpart that accounts only for the subgrid variation of  $q_c$ , especially at cloud top. Although this study is based on limited cases, it suggests that the subgrid variations of  $N_c$  and its correlation with  $q_c$  both need to be considered for an accurate simulation of the autoconversion process in GCMs.

Deleted: ,

Deleted: makes

Deleted: has a robust decreasing trend from cloud base to cloud top. Because the autoconversion process is most important at the cloud top, this vertical dependence of EF should be taken into consideration in the GCM parametrization scheme....

56

57 **1. Introduction**

58 Marine boundary layer (MBL) clouds cover about 1/5 of Earth's surface and play an important  
 59 role the climate system (Wood, 2012). A faithful simulation of MBL clouds in the global climate  
 60 model (GCM) is critical for the projection of future climate (Bony and Dufresne, 2005; Bony et  
 61 al., 2015; Boucher et al., 2013) and understanding of aerosol-cloud interactions (Carslaw et al.,  
 62 2013; Lohmann and Feichter, 2005). Unfortunately, it turns out to be an extremely challenging  
 63 task. Among others, an important reason is that many physical processes in MBL clouds occur on  
 64 spatial scales that are much smaller than the typical resolution of GCMs.

65 Of particular interest in this study is the warm rain processes that play an important role in  
 66 regulating the lifetime, water budget, and therefore integrated radiative effects of MBL clouds. In  
 67 the bulk cloud microphysics schemes that are widely used in GCMs (Morrison and Gettelman,  
 68 2008), continuous cloud particle spectrum is often divided into two modes. Droplets smaller than  
 69 the "separation size"  $r^*$  are classified into the cloud mode, which is described by two moments of  
 70 droplet size distribution (DSD), the droplet number concentration  $N_c$  (0<sup>th</sup> moment of DSD) and  
 71 droplet liquid water content  $q_c$  (proportional to the 3<sup>rd</sup> moment). Droplets larger than  $r^*$  are  
 72 classified into a precipitation mode (drizzle or rain), with properties denoted by drop concentration  
 73 and water content ( $N_r$  and  $q_r$ ). In a bulk microphysics scheme, the transfer of mass from the cloud  
 74 to rain modes as a result of the collision-coalescence process is separated into two terms,  
 75 autoconversion and accretion:  $\left(\frac{\partial q_r}{\partial t}\right)_{coal} = \left(\frac{\partial q_r}{\partial t}\right)_{auto} + \left(\frac{\partial q_r}{\partial t}\right)_{acc}$ . Autoconversion is defined as the  
 76 rate of mass transfer from the cloud to rain mode due to the coalescence of two cloud droplets with  
 77  $r < r^*$ . Accretion is defined as the rate of mass transfer due to the coalescence of a rain drop with  
 78  $r > r^*$  with a cloud droplet. A number of autoconversion and accretion parameterizations have

**Deleted:** Marine boundary layer (MBL) clouds cover about 1/5 of Earth's surface and play an important role the climate system (Wood, 2012). A faithful simulation of MBL clouds in the global climate model (GCM) is critical for the projection of future climate (Bony and Dufresne, 2005; Bony et al., 2015; Boucher et al., 2013) and understanding of aerosol-cloud interactions (Carslaw et al., 2013; Lohmann and Feichter, 2005). Unfortunately, it turns out to be an extremely challenging task. Among others, an important reason is that many physical processes in MBL clouds occur at the spatial scales much smaller than the typical resolution of GCMs, making the simulation of these processes in GCMs highly challenging. ¶  
 Of particular interest in this study is the warm rain process

**Deleted:** (Morrison and Gettelman, 2008)

94 been developed, formulated either through numerical fitting of droplet spectra obtained from bin  
 95 microphysics LES or parcel model (Khairoutdinov and Kogan, 2000), or through an analytical  
 96 simplification of the collection kernel to arrive at expressions that link autoconversion and  
 97 accretion with the bulk microphysical variables (Liu and Daum, 2004). For example, a widely used  
 98 scheme developed by Khairoutdinov and Kogan (2000) (“KK scheme” hereafter) relates the  
 99 autoconversion with  $N_c$  and  $q_c$  as follows:

$$\left(\frac{\partial q_r}{\partial t}\right)_{auto} = f_{auto}(q_c, N_c) = C q_c^{\beta_q} N_c^{\beta_N}, \quad (1)$$

100 where  $q_c$  and  $N_c$  have units of  $\text{kg kg}^{-1}$  and  $\text{cm}^{-3}$ , respectively; the parameter  $C = 1350$ , and the  
 101 two exponents  $\beta_q = 2.47$ ,  $\beta_N = -1.79$  are obtained through a nonlinear regression between the  
 102 variables  $q_c$  and  $N_c$  and the autoconversion rate derived from large-eddy simulation (LES) with  
 103 bin-microphysics spectra.

104 Having a highly accurate microphysical parameterization — specifically, highly accurate  
 105 local microphysical process rates — is not sufficient for an accurate simulation of warm-rain  
 106 processes in GCMs. Clouds can have significant structures and variations at the spatial scale much  
 107 smaller than the typical grid size of GCMs (10 ~ 100 km) (Barker et al., 1996; e.g., Cahalan and  
 108 Joseph, 1989; Lebsock et al., 2013; Wood and Hartmann, 2006; Zhang et al., 2019). Therefore,  
 109 GCMs need to account for these subgrid-scale variations in order to correctly calculate grid-mean  
 110 autoconversion and accretion rates. Pincus and Klein (2000) nicely illustrate this dilemma. Given  
 111 subgrid-scale variability represented as a distribution  $P(x)$  of some variable  $x$ , for example the  $q_c$   
 112 in Eq. (1), a grid-mean process rate is calculated as  $\langle f(x) \rangle = \int f(x)P(x)dx$ , where  $f(x)$  is the  
 113 formula for the local process rate. For nonlinear process rates such as autoconversion and accretion,  
 114 the grid-mean process rates calculated from the subgrid-scale variability does not equal the process  
 115 rate calculated from the grid-mean value of  $x$ , i.e.,  $\langle f(x) \rangle \neq f(\langle x \rangle)$ . Therefore, calculating

Deleted: (Khairoutdinov and Kogan, 2000)

Deleted: (Liu and Daum, 2004).

Deleted: (2000)

Deleted: (Barker et al., 1996; e.g., Cahalan and Joseph, 1989; Lebsock et al., 2013; Wood and Hartmann, 2006; Zhang et al., 2019)...

autoconversion and accretion from grid-mean quantities introduces biases arising from subgrid-scale variability. To take this effect into account, a parameter  $E$  is often introduced as part of the parameterization such that  $\langle f(x) \rangle = E \cdot f(\langle x \rangle)$ . Following the convention of previous studies,  $E$  is referred to as the “enhancement factor” (EF) here. Given the autoconversion parameterization scheme, the magnitude of EF is primarily determined by cloud horizontal variability within a GCM grid. Unfortunately, because most GCMs do not resolve subgrid cloud variation, the value of EF is often simply assumed to be a constant for the lack of better options. In the previous generation

of GCMs, the EF for KK autoconversion scheme due to subgrid  $q_c$  variation is often simply assumed to be a constant. For example, in the widely used Community Atmosphere Model (CAM) version 5 (CAM5) the EF for autoconversion is assumed to be 3.2 (Morrison and Gettelman, 2008).

A number of studies have been carried out to better understand the horizontal variations of cloud microphysics in MBL cloud and the implications for warm rain simulations in GCMs. Most of these studies have been focused on the subgrid variation of  $q_c$ . Morrison and Gettelman (2008) and several later studies (Boutle et al., 2014; Hill et al., 2015; Lebsock et al., 2013; Zhang et al., 2019) showed that the subgrid variability  $q_c$  and thereby the EF are dependent on cloud regime and cloud fraction ( $f_c$ ). They are generally smaller over the closed-cell stratocumulus regime with higher  $f_c$  and larger over the open-cell cumulus regime that often has a relatively small  $f_c$ . The subgrid variance of  $q_c$  is also dependent on the horizontal scale ( $L$ ) of a GCM grid. Based on the combination of in situ and satellite observations, Boutle et al. (2014) found that the subgrid  $q_c$  variance first increases quickly with  $L$  when  $L$  is below about 20 km, then increases slow and seems to approach a asymptotic value for larger  $L$ . Similar spatial dependence is also reported in Huang et al. (2014), Huang and Liu (2014), Xie and Zhang (2015), and Wu et al. (2018) which are based on the ground radar retrievals from the Department of Energy (DOE) Atmospheric

**Deleted:** The

**Deleted:** 3.2 in the two-moment scheme by Morrison and Gettelman (2008), which is employed

**Deleted:** Morrison and Gettelman (2008) and several later studies (Boutle et al., 2014; Hill et al., 2015; Lebsock et al., 2013; Zhang et al., 2019) showed that the subgrid variability  $q_c$  and thereby the EF are dependent on cloud regime and cloud fraction ( $f_c$ ). They are generally smaller over the closed-cell stratocumulus regime with higher  $f_c$  and larger over the open-cell cumulus regime that often has a relatively small  $f_c$ . The subgrid variance of  $q_c$  is also dependent on the horizontal scale ( $L$ ) of a GCM grid. Based on the combination of in situ and satellite observations, Boutle et al. (2014) found that the subgrid  $q_c$  variance first increases quickly with  $L$  when  $L$  is below about 20 km, then increases slow and seems to approach a asymptotic value for larger  $L$ . Similar spatial dependence is also reported in Huang et al. (2014), Huang and Liu (2014), Xie and Zhang (2015), and Wu et al. (2018) which are based on the ground radar retrievals from the Department of Energy (DOE) Atmospheric Radiation Measurement (ARM) sites. The cloud-regime and horizontal-scale dependences have inspired a few studies to parameterize the subgrid  $q_c$  variance as a function of either  $f_c$  or  $L$  or a combination of the two (e.g., Ahlgrimm and Forbes, 2016; Boutle et al., 2014; Hill et al., 2015; Xie and Zhang, 2015; Zhang et al., 2019)....

172 Radiation Measurement (ARM) sites. The cloud-regime and horizontal-scale dependences have  
 173 inspired a few studies to parameterize the subgrid  $q_c$  variance as a function of either  $f_c$  or  $L$  or a  
 174 combination of the two (e.g., Ahlgrimm and Forbes, 2016; Boutle et al., 2014; Hill et al., 2015;  
 175 Xie and Zhang, 2015; Zhang et al., 2019). Inspired by these studies, several latest-generation  
 176 GCMs have adopted the cloud-regime dependent and scale-aware parameterization schemes to  
 177 account for the subgrid variability of  $q_c$  and thereby the EF (Walters et al., 2019).

178 However, the aforementioned studies have an important limitation. They consider only the  
 179 impacts of subgrid  $q_c$  variations on the EF but ignore the impacts of subgrid variation of  $N_c$  and  
 180 its covariation with  $q_c$ . Based on cloud fields from large-eddy simulation, Larson and Griffin  
 181 (2013) and later Kogan and Mechem (2014; 2016) elucidated that it is important to consider the  
 182 covariation of  $q_c$  and  $N_c$  to derive a physically complete and accurate EF for the autoconversion  
 183 parameterization. Lately, on the basis of MBL cloud observations from the Moderate Resolution  
 184 Imaging Spectroradiometer (MODIS) Zhang et al. (2019) (hereafter referred to as Z19) elucidate  
 185 that the subgrid variation of  $N_c$  tends to further increase the EF for the autoconversion process in  
 186 addition to the EF due to  $q_c$  variation. The effect of  $q_c$ - $N_c$  covariation on the other hand depends  
 187 on the sign of the  $q_c$ - $N_c$  correlation. A positive  $q_c$ - $N_c$  correlation would lead to an EF <1 that  
 188 partly offsets the effects of  $q_c$  and  $N_c$  variations. Although Z19 shed important new light on the  
 189 EF problem for the warm rain process, their study also suffers from limitations due to the use of  
 190 satellite remote sensing data. First, as a passive remote sensing technique, MODIS cloud product  
 191 can only retrieve the column-integrated cloud optical thickness and the cloud droplet effective  
 192 radius at cloud top, from which the column-integrated cloud liquid water path (LWP) is estimated.  
 193 As a result of using LWP, instead vertically resolved observations the vertical dependence of the  
 194  $q_c$  and  $N_c$  horizontal variabilities are ignored in Z19. Second, the  $N_c$  retrieval from MODIS is

Deleted: The

Deleted: (2013)

Deleted: (2014; 2016)

Deleted: (2019)

199 based on several important assumptions, which can lead to large uncertainties (see review by  
200 [\(Grosvenor et al., 2018\)](#) ). Furthermore, MODIS cloud retrieval product is known to suffer from  
201 several inherent uncertainties, such as the three-dimensional radiative effects([e.g., Zhang and](#)  
202 [Platnick, 2011; Zhang et al., 2012; 2016](#)), which in turn can lead to large uncertainties in the  
203 estimated EF.

Deleted: (Grosvenor et al., 2018) ).

Deleted: (e.g., Zhang and Platnick, 2011; Zhang et al., 2012; 2016)...

204 This study is a follow up of Z19. To overcome the limitations of satellite observations, we  
205 use the in situ measurements of MBL cloud from a recent DOE field campaign, the Aerosol and  
206 Cloud Experiments in the Eastern North Atlantic (ACE-ENA), to investigate the subgrid variations  
207 of  $q_c$  and  $N_c$ , as well as their covariation, and the implications for the simulation of autoconversion  
208 simulation in GCMs. A main focus of this investigation is to understand the vertical dependence  
209 of the  $q_c$  and  $N_c$  horizontal variations within the MBL clouds. This aspect has been neglected in  
210 Z19 as well as most previous studies ([Boutle et al., 2014; Lebsock et al., 2013; Xie and Zhang,](#)  
211 [2015](#)). A variety of microphysical processes, such as adiabatic growth, collision-coalescence,  
212 entrainment mixing, can influence the vertical structure of MBL clouds. At the same time, these  
213 processes also vary horizontally at the subgrid scale of GCMs. As a result, the horizontal variations  
214 of  $q_c$  and  $N_c$ , as well as their covariation, and therefore the EFs may depend on the vertical location  
215 inside the MBL clouds. It is important to understand this dependence for several reasons. First, the  
216 warm rain process is usually initialized at cloud top where the autoconversion process of the cloud  
217 droplets gives birth to embryo drizzle drops. The accretion process is, on the other hand, more  
218 important in the lower part of the cloud([Wood, 2005b](#)). Thus, a better understanding of the vertical  
219 dependence of horizontal variations of  $q_c$  and  $N_c$  inside of MBL cloud could help us understand  
220 how the EF should be modeled in the GCMs, [for both autoconversion and accretion](#). Second, a  
221 good understanding of the vertical dependence of  $q_c$  and  $N_c$  variation inside of MBL clouds will

Deleted: (Boutle et al., 2014; Lebsock et al., 2013; Xie and Zhang, n.d.).

Deleted: (Wood, 2005b)

Deleted: .

also help us understand the limitations in the previous studies, such as Z19, that use the column-integrated products for the study of EF. Finally, this investigation may also be useful for modeling other processes, such as aerosol-cloud interactions, in the GCMs.

Therefore, our main objectives in this study are to: 1) better understand the horizontal variations of  $q_c$  and  $N_c$ , their covariation, and the dependence on vertical height in MBL clouds; 2) elucidate the implications for the EF of the autoconversion parameterization in GCMs. The rest of the paper is organized as follows: we will describe the data and observations used in this study in Section 2 and explain how we select the cases from the ACE-ENA campaign for our study in Section 3. We will present cases studies in Section 4 and 5. Finally, the results and findings from this study will be summarized and discussed in Section 6.

239

## 2. Data and Observations

The data and observations used for this study are from two main sources: the in-situ measurements from the ACE-ENA campaign and the ground-based observations from the ARM ENA site. The ENA region is characterized by persistent subtropical MBL clouds that are influenced by different seasonal meteorological conditions and a variety of aerosol sources (Wood et al., 2015). A modeling study by Carslaw et al. (2013) found the ENA to be one of regions over the globe with the largest uncertainty of aerosol indirect effect. As such, the ENA region attracted substantial attention over the past few decades for aerosol-cloud interaction studies. From April 2009 to December 2010 the DOE ARM program deployed its ARM Mobile Facility (AMF) to the Graciosa Island (39.09°N, 28.03°W) for a measurement field campaign targeting the properties of cloud, aerosol and precipitation in the MBL (CAP-MBL) in the Azores region of ENA (Wood et al., 2015). The measurements from the CAP-MBL campaign have proved highly useful for a

Deleted: as well as

Deleted: in MBL clouds, in particular their

Deleted: the

Deleted: cloud

Deleted: The ENA region is characterized by persistent subtropical MBL clouds that are influenced by different seasonal meteorological conditions and a variety of aerosol sources (Wood et al., 2015). A modeling study by Carslaw et al. (2013) found the ENA to be one of regions over the globe with the largest uncertainty of aerosol indirect effect. As such, the ENA region attracted substantial attention over the past few decades for aerosol-cloud interaction studies. From April 2009 to December 2010 the DOE ARM program deployed its ARM Mobile Facility (AMF) to the Graciosa Island (39.09°N, 28.03°W) for a measurement field campaign targeting the properties of cloud, aerosol and precipitation in the MBL (CAP-MBL) in the Azores region of ENA (Wood et al., 2015). The measurements from the CAP-MBL campaign have proved highly useful for a variety of purposes, from understanding the seasonable variability of clouds and aerosols in the MBL of the ENA region (Dong et al., 2014; Rémillard et al., 2012) to improving cloud parameterizations in the GCMs (Zheng et al., 2016) and to validating the space-borne remote sensing products of MBL clouds (Zhang et al., 2017). The success of the CAP-MBL revealed that the ENA has an ideal mix of conditions to study the interactions of aerosols and MBL clouds. In 2013 a permanent measurement site is established by the ARM program on Graciosa Island as its newest permanent atmospheric observatories, also known as the ENA site (Voyles and Mather, 2013)

variety of purposes, from understanding the seasonal variability of clouds and aerosols in the MBL of the ENA region (Dong et al., 2014; Rémillard et al., 2012) to improving cloud parameterizations in the GCMs (Zheng et al., 2016), to validating the space-borne remote sensing products of MBL clouds (Zhang et al., 2017). The success of the CAP-MBL revealed that the ENA has an ideal mix of conditions to study the interactions of aerosols and MBL clouds. In 2013 a permanent measurement site was established by the ARM program on Graciosa Island, and is typically referred to as the ENA site (Voyles and Mather, 2013).

## 2.1. In situ measurements from the ACE-ENA campaign

The Aerosol and Cloud Experiments in ENA (ACE-ENA) project was “*motivated by the need for comprehensive in situ characterizations of boundary-layer structure and associated vertical distributions and horizontal variabilities of low clouds and aerosol over the Azores*” (Wang et al., 2016). The ARM Aerial Facility (AAF) Gulfstream-1 (G-1) aircraft was deployed during two intensive measurement periods (IOPs), the summer 2017 IOP from June 21 to July 20, 2017 and the winter 2018 IOP from January 15 to February 18, 2018. Over 30 research flights (RF) were carried out during the two IOPs around the ARM ENA site on Graciosa Island that sampled a large variety of cloud and aerosol properties along with the meteorological conditions.

Table 1 summarizes the in-situ measurements from the ACE-ENA campaign used in this study. The location and velocity of G1 aircraft, and the environment meteorological conditions during the flight (temperature, humidity, and wind velocity) are taken from Aircraft-Integrated Meteorological Measurement System 20-Hz (AIMMS-20) dataset (Beswick et al., 2008). The size distribution of cloud droplets, and the corresponding  $q_c$  and  $N_c$  are obtained from the fast cloud droplet probe (FCDP) measurement. The FCDP measures the concentration and size of cloud droplets in the diameter size range from 1.5 to 50  $\mu\text{m}$  in 20 size bins with an overall uncertainty

Deleted: (Wang et al., 2016)

Formatted: Font: 12 pt, Not Italic

Deleted: Table 1

Deleted: (Beswick et al., 2008)

309 of size around  $3\text{ }\mu\text{m}$  (Lance et al., 2010; SPEC, 2019). Following previous studies (Wood, 2005a),  
 310 we adopt a  $r^* = 20\text{ }\mu\text{m}$  as the threshold to separate cloud droplets from drizzle drops, i.e., drops  
 311 with  $r < r^*$  are considered as cloud droplets. After the separation, the  $q_c$  and  $N_c$  are derived from  
 312 the FCDP droplet size distribution measurements. As an evaluation, we compared our FCDP-  
 313 derived  $q_c$  results with the direct measurements of  $q_c$  from the multi-element water content system  
 314 (WCM-2000; (Matthews and Mei, n.d.)) also flown during the ACE-ENA and found a reasonable  
 315 agreement (e.g., biases within 20%). We also performed a few sensitivity tests in which we  
 316 perturbed the value of  $r^*$  from  $15\text{ }\mu\text{m}$  up to  $50\text{ }\mu\text{m}$ . The perturbation shows little impact on the  
 317 results shown in sections 4 and 5. The cloud droplet spectrum from the FCDP is available at a  
 318 frequency of  $10\text{ Hz}$ , which is used in this study. We have also done a sensitivity study, in which  
 319 we averaged the FCDP data to  $1\text{ Hz}$  and got almost identical results. Since the typical horizontal  
 320 speed of the G-1 aircraft during the in-cloud leg is about  $100\text{ m s}^{-1}$ , the spatial sampling rate these  
 321 instruments is on the order of  $10\text{ m}$  for the FCDP at  $10\text{ Hz}$ .

## 322 2.2. Ground observations from ARM ENA site

323 In addition to the in-situ measurements, ground measurements from the ARM ENA site  
 324 are also used to provide ancillary data for our studies. In particular, we will use the Active Remote  
 325 Sensing of Cloud Layers product (ARSCL; (Clothiaux et al., 2000; Kollias et al., 2005) which  
 326 blends radar observations from the Ka-band ARM zenith cloud radar (KAZR), micropulse lidar  
 327 (MPL), and the ceilometer to provide information on cloud boundaries and the mesoscale structure  
 328 of cloud and precipitation. The ARSCL product is used to specify the vertical location of the G1  
 329 aircraft and thereby the in-situ measurements with respect to the cloud boundaries, i.e., cloud base  
 330 and top (see example in Figure 1). In addition, the radar reflectivity observations from KAZR,  
 331 alone with in situ measurements, are used to select the precipitating cases for our study. Note that

Deleted: (Lance et al., 2010; SPEC, 2019).

Deleted: (Wood, 2005a)

Deleted: )

Deleted: an excellent

Deleted: .

Deleted: couple of

Deleted: by  $\pm 5$

Deleted: .

Deleted: (Clothiaux et al., 2000; Kollias et al., 2005)

Deleted: Figure 1

the ARSCL product is from the vertically pointing instruments, which sometimes are not collocated with the in-situ measurements from G1 aircraft. As explained later in the next section, only those cases with a reasonable collocation are selected for our study.

### 3. Case selections

#### 3.1. ACE-ENA flight pattern

The section provides a brief overview of the G1 aircraft flight patterns during the ACE-ENA and explains the method for cases selections for our study using the July 18, 2017 RF as an example. As shown in Table 2, a variety of MBL conditions were sampled during the two IOPs of the ACE-ENA campaign, from mostly clear-sky to thin stratus and drizzling stratocumulus. The basic flight patterns of G1 aircraft in the ACE-ENA included spirals to obtain vertical profiles of aerosol and clouds, and legs at multiple altitudes, including below cloud, inside cloud, at the cloud top, and in the free troposphere. As an example, Figure 1a shows the horizontal location of the G1 aircraft during the July 18, 2017 RF which is the “golden case” for our study as explained in the next section. The corresponding vertical track of the aircraft is shown in Figure 1b overlaid on the reflectivity curtain of ground based KAZR. In this RF, the G1 aircraft repeated multiple times of horizontal level runs in a “V” shape at different vertical levels inside, above and below the MBL (see Figure 1b). The lower tip of the “V” shape is located at the ENA site on Graciosa island. The average wind in the upper MBL (i.e., 900 mb) is approximately Northwest. So, the west side of the V-shape horizontal level runs is along the wind and the east side across the wind. Note that the horizontal velocity of the G1 aircraft is approximately  $100 \text{ m s}^{-1}$ . Since the duration of these selected “V” shape hlegs is between 580 s and 700 s, their total horizontal length is roughly 60 km, with each side of the “V” shape  $\sim 30 \text{ km}$ . These “V” shape horizontal level runs, with one side along and the other across the wind, are a common sampling strategy used in the ACE-ENA to

Deleted: Table 2

Deleted: In this study, we are interested in the RFs that encountered the drizzling stratocumulus clouds, since our objective is to understand the implications of subgrid cloud variation for the autoconversion process.

Deleted: Figure 1

Deleted: Figure 1

Deleted: Figure 1

Deleted: left

Deleted: right

Deleted: cross

Deleted: cross

377 observe the properties of aerosol and cloud at different vertical levels of the MBL. In our study we  
 378 use the vertical location of the G1 aircraft from the AIMMS to identify continuous horizontal flight  
 379 tracks which are referred to as the “hleg”. For the July 18, 2017 case, a total of 13 hlegs are  
 380 identified as shown in Figure 1b. Among them, the hleg 5, 6, 7, 8, 10, 11, and 12 are the seven V-  
 381 shape horizontal level runs inside the MBL cloud. Together they provide an excellent set of  
 382 samples of the MBL cloud properties at different vertical levels of a “virtual” GCM grid box of  
 383 about 30 km. As aforementioned, Boutle et al. (2014) found that the horizontal variance of  $q_c$   
 384 increases with the horizontal scale  $L$  slowly when  $L$  is larger than about 20 km. Therefore,  
 385 although the horizontal sampling of the selected hlegs is only about 30 km, the lessons learned  
 386 here could yield useful insights for larger GCM grid sizes. In addition to the hlegs, we also  
 387 identified the vertical penetration legs in each flight, referred to as the “vlegs”, from which we will  
 388 obtain the vertical structure of the MBL, along with the properties of cloud and aerosol.

### 389 3.2. Case selection

390 As illustrated in Figure 1, a and b for the July 18, 2017 RF, the criteria we used to select the  
 391 RF cases and the hlegs within the RF can be summarized as follows:

- 392 • The RF samples multiple continuous in-cloud hlegs at different vertical levels with the  
 393 horizontal length of at least 10 km and cloud fraction larger than 10% (i.e., the fraction of  
 394 a hleg with  $q_c > 0.01 \text{ g m}^{-3}$  must exceed 10% of the total length of that hleg). It is important  
 395 to note here that, unless otherwise specified, all the analyses of  $q_c$  and  $N_c$  are based on in-  
 396 cloud observations (i.e., in the regions with  $q_c > 0.01 \text{ g m}^{-3}$ ).
- 397 • Moreover, the selected hlegs must sample the same region (i.e., the same virtual GCM grid  
 398 box) repeatedly in terms of horizontal track but different vertical levels in terms of vertical  
 399 track. Take the July 18, 2017 case as an example. The hleg 5, 6, 7, 8 follow the same “V”

Deleted: Figure 1

Deleted: Figure 1

Deleted: criteria

Deleted: <#>The RF encounters precipitating MBL clouds according to both pilot report and radar reflectivity observations from the ground-based KAZR. ¶

Deleted: <#>)

shape horizontal track (see [Figure 1a](#)) but sample different vertical levels of the MBL clouds (see [Figure 1b](#)). Such hlegs provide us the horizontal sampling needed to study the subgrid horizontal variations of the cloud properties and, at the same time, the chance to study the vertical dependence of the horizontal cloud variations.

- Finally, the RF needs to have at least one vleg and the cloud boundary derived from the vleg is largely consistent with that derived from the ground-based measurements. This requirement is to ensure that the vertical locations of the selected hlegs with respect to cloud boundaries can be specified. For example, as shown in [Figure 1b](#) according to the ground-based observations, the hlegs 5 and 10 of July 18, 2017 case are close to cloud base, while hlegs 8 and 12 close to cloud top (see also [Figure 4](#)).

The above requirements together pose a strong constraint on the observation. Fortunately, thanks to the careful planning of the RF which had already taken studies like ours into consideration, we are able to select a total of [seven](#) RF cases as summarized in [Table 3](#). [The plots of the flight tracks and ground-based radar observations for the six other RF cases are provided in the supplementary material \(Figure S1—S6\)](#). We will first focus on the “golden case—July 18, 2017 RF and then investigate if the lessons learned from the July 18, 2017 RF also apply to the other three cases.

#### 4. A study of the July 18, 2017 case

##### 4.1. Horizontal and vertical variations of cloud microphysics

On July 18, 2017, the North Atlantic is controlled by the Icelandic low to the north and the Azores high to the south (see [Figure 2b](#)), which is a common pattern of large-scale circulation during the summer season in this region ([Wood et al., 2015](#)). The Azores is at the southern tip of the cold air sector of a frontal system where the fair-weather low-level stratocumulus clouds are dominant (see satellite image in [Figure 2a](#)). The RF on this day started around 8:30 UTC and ended

Deleted: Figure 1

Deleted: Figure 1

Deleted: Figure 1

Deleted: Figure 4

Deleted: four

Deleted: Table 3

Deleted: Figure 2

Deleted: (Wood et al., 2015)

Deleted: Figure 2

439 around 12 UTC. As explained in the previous section, we selected 7 hlegs from this RF that  
 440 horizontally sampled the same region repeatedly in a similar “V” shaped track but vertically at  
 441 different levels. The radar reflectivity observation from the ground based KAZR during the same  
 442 period peaks around 10 dBZ indicating the presence of significant drizzle inside the MBL clouds.

443 Among the 7 selected hlegs, the hlegs 5, 6, 7 and 8 constitute one set of 4 consecutive “V”  
 444 shape tracks, with hlegs 5 close to cloud base and hleg 8 close to cloud top. The hlegs 10,11 and  
 445 12 are another set of consecutive “V” shape tracks with hlegs 10 and 12 close to cloud base and  
 446 top, respectively (see Figure 1). Using  $q_c > 0.01 \text{ gm}^{-3}$  as a threshold for cloud, the cloud fraction  
 447 ( $f_c$ ) of all these hlegs is close to unity (i.e., overcast), except for the two hlegs close to cloud base  
 448 ( $f_c=46\%$  for hleg 5 and  $f_c=51\%$  for hleg 10). The  $q_c$  and  $N_c$  derived from the in situ FCDP  
 449 measurements for these selected hleg are plotted in Figure 3, as a function of UTC time. It is evident  
 450 from Figure 3, that both  $q_c$  and  $N_c$  have significant horizontal variations. At cloud base (see Figure  
 451 3d for hleg 5 and Figure 3g for hleg 10) the  $q_c$  varies from  $0.01 \text{ gm}^{-3}$  (i.e., the lower threshold) up  
 452 to about  $0.4 \text{ gm}^{-3}$  and the  $N_c$  from  $25 \text{ cm}^{-3}$  up to  $150 \text{ cm}^{-3}$ , with the mean in-cloud values around  
 453  $0.08 \text{ gm}^{-3}$  and  $65 \text{ cm}^{-3}$ , respectively. Such strong variations of cloud microphysics could be  
 454 contributed by a number of factors. One can see from the ground radar and lidar observations in  
 455 Figure 1b that the height of cloud base varies significantly. As a result, the horizontal legs may not  
 456 really sample the cloud base. In addition, the variability in updraft at cloud base could lead to the  
 457 variability in the activation and growth of cloud condensation nuclei (CCN). In the middle of the  
 458 MBL cloud, i.e., hleg 6 (Figure 3c), 7 (Figure 3b) and 11 (Figure 3f), the mean value of  $q_c$  is  
 459 significantly larger than that of cloud base hlegs while the variability is reduced. The mean value  
 460 of  $q_c$  keeps increasing toward cloud top to  $\sim 0.73 \text{ gm}^{-3}$  in hleg 8 (Figure 3a) and to  $\sim 0.53 \text{ gm}^{-3}$  in

Deleted: are

Deleted: Figure 1

Deleted: Figure 3

Deleted: Figure 3

Deleted: Figure 3

Deleted: Figure 3

Deleted: Figure 1

Deleted: cloud

Deleted: ).

Deleted: Figure 3

Deleted: Figure 3

Deleted: Figure 3

Deleted: Figure 3

hleg 12 (Figure 3e), respectively. In contrast, the horizontal variability of  $q_c$  seems to increase in comparison with those observed in mid-level hlegs.

To obtain a further understanding of the vertical variations of cloud microphysics, we analyzed the cloud microphysics observations from the two green-shaded vlegs 1 and 3 in Figure 1b. The vertical profile of the mean  $q_c$  and  $N_c$  from these two vlegs are shown in Figure 4a and Figure 4b, respectively, with over-plotted the mean and standard deviation of the  $q_c$  and  $N_c$  derived from the 7 selected hlegs. Overall, the vertical profiles of the  $q_c$  and  $N_c$  are qualitatively aligned with the classic adiabatic MBL cloud structure (Brenguier et al., 2000; Martin et al., 1994). That is, the  $N_c$  remains relatively a constant (see Figure 4b) while the  $q_c$  increases approximately linearly with height from cloud base upward as a result of condensation growth (see Figure 4a), except for the very top of the cloud, i.e., the entrainment zone where the dry air entrained from the above mixes with the humid cloudy air in the MBL. In previous studies, a so-called inverse relative variance,  $\nu$ , is often used to quantify the subgrid variations of cloud microphysics. It is defined as follows

$$\nu_X = \frac{\langle X \rangle^2}{\sigma_X^2}, \quad (2)$$

where  $X$  is either  $q_c$  (i.e.,  $\nu_X = \nu_{q_c}$ ) or  $N_c$  (i.e.,  $\nu_X = \nu_{N_c}$ ) (Barker et al., 1996; Lebsock et al., 2013; Zhang et al., 2019).  $\langle X \rangle$  and  $\sigma_X$  are the mean value and standard deviation of  $X$ , respectively. As such the smaller the  $\nu$  value the larger the horizontal variation of  $X$  in comparison with the mean value. As shown in Figure 4c, the  $\nu_{q_c}$  and  $\nu_{N_c}$  derived from the selected hlegs follow a similar vertical pattern: they both increase first from cloud base upward and then decrease in the entrainment zone, with the turning point somewhere around 1 km (i.e., around hleg 7 and 11). It indicates that both  $q_c$  and  $N_c$  have significant horizontal variabilities at cloud base which may be a combined result of horizontal fluctuations of dynamics (e.g., updraft) and thermodynamics (e.g.,

Deleted: Figure 3

Deleted: Figure 1

Deleted: Figure 4

Deleted: Figure 4

Deleted: (Brenguier et al., 2000; Martin et al., 1994)

Deleted: Figure 4

Deleted: Figure 4

Deleted: Figure 4

504 temperature and dynamics), as well as horizontal variations of aerosols. The horizontal variabilities  
 505 of both  $q_c$  and  $N_c$  both decrease upward toward cloud top until the entrainment zone where both  
 506 variabilities increase again.

507 So far, in all the analyses above the variations of  $q_c$  and  $N_c$  have been considered  
 508 separately and independently. As pointed out in several previous studies, the co-variation of  $q_c$   
 509 and  $N_c$  could have an important impact on the EF for the autoconversion process in GCMs (*Kogan*  
 510 *and Mechem, 2016; Larson and Griffin, 2013; Zhang et al., 2019*). This point will be further  
 511 elucidated in detail in the next section. *Figure 5* shows the joint distributions of  $q_c$  and  $N_c$  for the  
 512 7 selected hlegs and the corresponding linear correlation coefficients as a function of height are  
 513 shown in *Figure 4d*. For the sake of reference, the linear correlation coefficient between  $\ln(q_c)$   
 514 and  $\ln(N_c)$ , i.e., the  $\rho_L$  that will be introduced later in Eq. (4), is also plotted in *Figure 4d*.  
 515 Looking first at the hlegs 10, 11 and 12, i.e., the 2<sup>nd</sup> group of consecutive “V” shape legs, there is  
 516 a clear increasing trend of the correlation between  $q_c$  and  $N_c$  from cloud bottom ( $\rho = 0.75$  for  
 517 hleg 10) to cloud top ( $\rho = 0.95$  for hleg 12). The picture based on the hlegs 5, 6, 7, and 8 is more  
 518 complex. As shown in *Figure 5*, the joint distributions of  $q_c$  and  $N_c$  of hleg 6 (*Figure 5b*), hleg 7  
 519 (*Figure 5c*) and, to a less extent, hleg 8 (*Figure 5d*) all exhibit a clear bimodality. Further analysis  
 520 reveals that each of the two modes in these bimodal distributions approximately corresponds to  
 521 one side of the “V” shape track. *To illustrate this, the east side (i.e., across-wind) of the hleg is*  
 522 *shaded in yellow in Figure 3.* It is intriguing to note that the  $N_c$  from the *east* side of the hleg are  
 523 systematically larger than those from the *west* side, while their  $q_c$  values are largely similar. *It is*  
 524 *unlikely that the bimodality is caused by the along-wind and across-wind difference between the*  
 525 *two sides of the “V” shape track. It is most likely just a coincidence. On the other hand, the bimodal*

Deleted: (*Kogan and Mechem, 2016; Larson and Griffin, 2013; Zhang et al., 2019*)...

Deleted: Figure 5

Deleted: Figure 4

Deleted: (4)

Deleted: Figure 4

Deleted: Figure 5

Deleted: Figure 5

Deleted: Figure 5

Deleted: Figure 5

Deleted: As aforementioned, for all the selected 7 “V” shape hlegs, the left side is along the wind and the right side across the wind (see Figure 1). To illustrate this difference, the across-wind side

Deleted: Figure 3

Deleted: across-wind

Deleted: along-wind

joint distribution between  $q_c$  and  $N_c$  is “real” which could be a result of subgrid variations of updraft, precipitation and/or aerosols.

As a result of the bimodality of  $N_c$ , the correlation coefficients between  $q_c$  and  $N_c$  is significantly smaller for the hlegs 6 ( $\rho = 0.22$ ) and 7 ( $\rho = 0.31$ ) in comparison with other hlegs.

However, if the two sides of the “V” shape tracks are considered separately, then the  $q_c$  and  $N_c$  become more correlated, except for the east side of hleg 6 which still exhibits to some degree a bimodal joint distribution of  $q_c$  and  $N_c$ . In spite of the bimodality, there is evidently a general increasing trend of the correlation between  $q_c$  and  $N_c$  from cloud base toward cloud top. At the cloud top, the  $q_c$  and  $N_c$  correlation coefficient can be as high as  $\rho = 0.95$  for hleg 12 (see Figure 5c). As explained in the next section, this close correlation between  $q_c$  and  $N_c$  has important implications for the simulation of autoconversion enhancement factor.

As a summary, the above phenomenological analysis of the July 18, 2017 RF reveals the following features of the horizontal and vertical variations of cloud microphysics. Vertically, the mean values of  $q_c$  and  $N_c$  qualitatively follow the adiabatic structure of MBL cloud, i.e.,  $q_c$  increases linear with height and  $N_c$  remains largely invariant above cloud base. Even though the joint distribution of  $q_c$  and  $N_c$  exhibits a bimodality in several hlegs, their correlation generally increases with height and can be as high as  $\rho = 0.95$  at cloud top. Horizontally, both  $q_c$  and  $N_c$  have a significant variability at cloud base, which tends to first decrease upward and then increase in the uppermost part of cloud close to the entrainment zone. Finally, we have to point out a couple of important caveats in the above analysis. First, as seen from Figure 1 the selected hlegs are sampled at different vertical locations and also at different time. For example, the hleg 5 at cloud base is more than 1 hour apart from the hleg 8 at cloud top (Figure 1a). As a result, the temporal evolution of clouds is a confounding factor and might be misinterpreted as vertical variations of

Deleted: this

Deleted:

Deleted: cross-wind

Deleted: distributions

Deleted:

Deleted: Figure 5

Deleted: explain

Deleted:

clouds. On the other hand, as shown below, we also observed similar vertical structure of  $q_c$  and  $N_c$  in other cases. It seems highly unlikely that the temporal evaluations of the clouds in all selected cases conspire to confound our results in the same way. Based on this consideration, we assume that the temporal evolution of clouds is an uncertainty that could lead to random errors but does not impact the overall vertical trend. The second caveat is that due to the very limited vertical sampling rate of hlegs (i.e., only 3-4 samples) we cannot possibly resolve the detailed vertical variation of  $v_{q_+}$ ,  $v_N$  and  $\rho$ . Although we have used the word “trend” in the above analysis, it should be noted that the vertical profile of these parameters may, but more likely may not, be linear. So, the word “trend” here indicates only the large pattern that can be resolved by the hlegs. Obviously these two caveats also apply to the analysis below of the EF which is also derived from the hlegs.

#### 4.2. Implications for the EF for the autoconversion rate parameterization

As explained in the introduction, in GCMs the autoconversion process is usually parameterized as a highly nonlinear function of  $q_c$  and  $N_c$ , e.g., the KK scheme in Eq. (1). In such parameterization, an EF is needed to account for the bias caused by the nonlinearity effect. A variety of methods have been proposed and used in the previous studies to estimate the EF (Larson and Griffin, 2013; Lebsock et al., 2013; Pincus and Klein, 2000; Zhang et al., 2019). The methods used in this study are based on Z19. Only the most relevant aspects are recapped here. Readers are referred to Z19 for detail.

If the subgrid variations of  $q_c$  and  $N_c$ , as well as their covariation, are known, then the EF can be estimated based on its definition as follows

$$E = \frac{\int_{N_{c,min}}^{\infty} \int_{q_{c,min}}^{\infty} q_c^{\beta_q} N_c^{\beta_N} P(q_c, N_c) dq_c dN_c}{\langle q_c \rangle^{\beta_q} \langle N_c \rangle^{\beta_N}}, \quad (3)$$

Deleted: (1)

Deleted: . In such parameterization, an EF is needed to account for the bias caused by the nonlinearity effect. A variety of methods have been proposed and used in the previous studies to estimate the EF (Larson and Griffin, 2013; Lebsock et al., 2013; Pincus and Klein, 2000; Zhang et al., 2019). The methods used in this study are based on Z19. Only the most relevant aspects are recapped here. Readers are referred to Z19 for detail. ¶ If the subgrid variations of  $q_c$  and  $N_c$ , as well as their covariation, are known, then the EF can be estimated based on its definition as follows¶

Deleted:  $E = \frac{\int_0^{\infty} \int_0^{\infty} q_c^{\beta_q} N_c^{\beta_N} P(q_c, N_c) dq_c dN_c}{\langle q_c \rangle^{\beta_q} \langle N_c \rangle^{\beta_N}},$

607 where  $\langle q_c \rangle$  and  $\langle N_c \rangle$  are the grid-mean value,  $P(q_c, N_c)$  is the joint probability density function  
 608 (PDF) of  $q_c$  and  $N_c$ .  $q_{c,min}$  and  $N_{c,min}$  are the lower limits of the in-cloud value (e.g.,  $q_{c,min}=0.01$   
 609  $\text{gm}^{-3}$ ). Some previous studies approximate the  $P(q_c, N_c)$  as a bivariate lognormal distribution as  
 610 follows:

$$P(q_c, N_c) = \frac{1}{2\pi q_c N_c \sigma_{q_c} \sigma_{N_c} \sqrt{1 - \rho_L^2}} \exp\left(-\frac{\zeta}{2}\right) \quad (4)$$

$$\zeta = \frac{1}{1 - \rho_L^2} \left[ \left( \frac{\ln q_c - \mu_{q_c}}{\sigma_{q_c}} \right)^2 - 2\rho \left( \frac{\ln q_c - \mu_{q_c}}{\sigma_{q_c}} \right) \left( \frac{\ln N_c - \mu_{N_c}}{\sigma_{N_c}} \right) + \left( \frac{\ln N_c - \mu_{N_c}}{\sigma_{N_c}} \right)^2 \right],$$

611 where  $\mu_X$  and  $\sigma_X$  are, respectively, the mean and standard deviation of  $\ln(X)$ , where  $X$  is either  
 612  $q_c$  or  $N_c$ .  $\rho_L$  is the linear correlation coefficient between  $\ln(q_c)$  and  $\ln(N_c)$ , (Larson and Griffin,  
 613 2013; Lebsock et al., 2013; Zhang et al., 2019). It should be noted here that  $\rho_L$  is fundamentally  
 614 different from  $\rho$  (i.e., the linear correlation coefficient between  $q_c$  and  $N_c$ ). On the other hand, we  
 615 found that for all the selected hlegs  $\rho$  and  $\rho_L$  are in an excellent agreement (see Figure 4d). In fact,  
 616  $\rho$  and  $\rho_L$  can be used interchangeably in the context of this study without any impact on the  
 617 conclusions. Nevertheless, interested readers may find more detailed discussion of the relationship  
 618 between  $\rho$  and  $\rho_L$  in Larson and Griffin (2013).

619 Substituting  $P(q_c, N_c)$  in Eq. (4) into Eq. (3) yields a formula for EF that consists of the  
 620 following three terms

$$E = E_q(v_{q_c}, \beta_q) \cdot E_N(v_{N_c}, \beta_N) \cdot E_{COV}(\rho_L, \beta_q, \beta_N v_{q_c}, v_{N_c}), \quad (5)$$

621 where  $E_q(v_{q_c}, \beta_q)$  corresponds to the enhancing effect of the subgrid variation of  $q_c$ , if  $q_c$  follows  
 622 a marginal lognormal distribution, i.e.,  $P(x) = \frac{1}{\sqrt{2\pi}\sigma} \exp\left(-\frac{(\ln x - \mu)^2}{2\sigma^2}\right)$ . It is a function of the  
 623 inverse relative variance  $v_q$  in Eq. (2) as follows:

Deleted: (Larson and Griffin, 2013; Lebsock et al., 2013; Zhang et al., 2019)...

Deleted: Figure 4

Deleted: (2013)

Formatted: Font: Not Italic

Deleted: (4)

Formatted: Font: Not Italic

Deleted: (3)

Formatted: Font: Not Italic

Deleted: (2)

$$E_q(v_{q_c}, \beta_q) = \left(1 + \frac{1}{v_{q_c}}\right)^{\frac{\beta_q^2 - \beta_q}{2}}. \quad (6)$$

631 Similarly, the  $E_N(v_{N_c}, \beta_N)$  below corresponds to the enhancing effect of the subgrid variation of  
 632  $N_c$ , if  $N_c$  follows a marginal lognormal distribution,

$$E_N(v_{N_c}, \beta_N) = \left(1 + \frac{1}{v_{N_c}}\right)^{\frac{\beta_N^2 - \beta_N}{2}}. \quad (7)$$

633 The third term  $E_{COV}(\rho_L, \beta_q, \beta_N, v_{q_c}, v_{N_c})$  in Eq. (5),

$$E_{COV}(\rho_L, \beta_q, \beta_N, v_{q_c}, v_{N_c}) = \exp(\rho_L \beta_q \beta_N \sigma_{q_c} \sigma_{N_c}), \quad (8)$$

634 corresponds to the impact of the co-variation of  $q_c$  and  $N_c$  on the EF. Because  $\beta_q > 0$  and  $\beta_N <$   
 635  $0$ , if  $q_c$  and  $N_c$  are negatively correlated (i.e.,  $\rho_L < 0$ ) then the  $E_{COV} > 1$  and acts as an enhancing  
 636 effect on the autoconversion rate computation. In contrast, if  $q_c$  and  $N_c$  are positively correlated  
 637 (i.e.,  $\rho_L > 0$ ), then the  $E_{COV} < 1$  which becomes a suppressing effect on the autoconversion rate  
 638 computation.

639 As aforementioned, most previous studies of the EF consider only the impact of subgrid  
 640  $q_c$  variation (i.e., only the  $E_q$  term). The impacts of subgrid  $N_c$  variation as well as its covariation  
 641 with  $q_c$  have been largely overlooked in observational studies, in which, the  $E_q$  is often derived  
 642 from the observed subgrid variation of  $q_c$  based on the definition of EF, i.e.,

$$E_q = \frac{\int_{q_{c,min}}^{\infty} q_c^{\beta_q} P(q_c) dq_c}{\langle q_c \rangle^{\beta_q}}, \quad (9)$$

643 where  $P(q_c)$  is the observed subgrid PDF of  $q_c$ . Alternatively,  $E_q$  have also been estimated from  
 644 the inverse relative variance  $v_q$  by assuming the subgrid variation of  $q_c$  to follow either the  
 645 lognormal distribution, in which case  $E_q$  is given in Eq. (6),

Deleted: (5)

Deleted:  $E_q = \frac{\int_0^{\infty} q_c^{\beta_q} P(q_c) dq_c}{\langle q_c \rangle^{\beta_q}},$

Deleted: (6)

Formatted: Font: Not Italic

Similar to  $E_N$ , if only the effect of subgrid  $N_c$  is considered, the corresponding  $E_N$  can be derived from the following two ways, one from the observed subgrid PDF  $P(N_c)$  based on the definition of EF, i.e.,

$$E_N = \frac{\int_{N_{cmin}}^{\infty} N_c^{\beta_N} P(N_c) dN_c}{\langle N_c \rangle^{\beta_N}}, \quad (10)$$

and the other based on Eq. (7) from the relative variance  $v_{N_c}$  by assuming the subgrid  $N_c$  variation to follow the lognormal distribution.

Now, we put the in-situ  $q_c$  and  $N_c$  observations from the selected hlegs in the theoretical framework of EF described above and investigate the following questions:

- 1) What is the (“observation-based”) EF derived based on Eq. (3) from the observed joint PDF  $P(q_c, N_c)$ ?
- 2) How well does the (“bi-logarithmic”) EF derived based on Eq. (5) by assuming that the covariation of  $q_c$  and  $N_c$  follows a bi-variate lognormal agree with the observation-based EF?
- 3) What is the relative importance of the  $E_q$ ,  $E_N$ , and  $E_{COV}$  terms in Eq. (5) in determining the value of EF?
- 4) What is the error of considering only  $E_q$  and omitting the  $E_N$  and  $E_{COV}$  terms?
- 5) How do the observation-based EFs from Eq. (3) and the  $E_q$ ,  $E_N$ ,  $E_{COV}$  terms vary with vertical height in cloud?

These questions are addressed in the rest of this section. Focusing first on the  $E_q$  in Figure 6a, the  $E_q$  derived from observation based on Eq. (9) (solid circle) shows a clear decreasing trend with height between cloud base at around 700 m to about 1 km, with value reduced from about 3 to about 1.2. Then, the value of  $E_q$  increases slightly in the cloud top hlegs 8 and 12. The  $E_q$  derived based on Eq. (6) by assuming lognormal distribution (open circle) has a very similar

Deleted:

Deleted:  $E_N = \frac{\int_0^{\infty} N_c^{\beta_N} P(N_c) dN_c}{\langle N_c \rangle^{\beta_N}},$

Deleted: (7)

Formatted: Font: Not Italic

Formatted: Font: Not Italic, Check spelling and grammar

Deleted: (3)

Deleted: (5)

Formatted: Font: Not Italic

Formatted: Font: Not Italic

Deleted: (5)

Formatted: Font: Not Italic, Check spelling and grammar

Deleted: (3)

Deleted: Figure 6

Formatted: Font: Not Italic

Deleted: (9)

Formatted: Font: Not Italic

Deleted: (6)

vertical pattern, although the value is slightly overestimated **on average by 0.07** in comparison with the observation-based result. The vertical pattern of  $E_q$  can be readily explained by how the subgrid variation of  $q_c$  in **Figure 4c**. The  $E_N$  derived from observation (solid triangle) in **Figure 6b** shows a similar vertical pattern as  $E_q$ , i.e., first decreasing with height from cloud base to about 1.2 km and then increasing with height in the uppermost part of cloud. The  $E_N$  derived based on Eq. **(7)** by assuming a lognormal distribution (open triangle) **significantly underestimate** the observation-based values **(mean bias of -4.3)**, especially at cloud base (i.e., hleg 5 and 10) and cloud top (i.e., hleg 8 and 12).

Using **hleg 10** as an example, we further investigated the cause for the error in lognormal-based EFs in comparison with those diagnosed from the observation. As shown in **Figure 7a** the observed  $q_c$  is slightly negatively skewed in logarithmic space by the small values. Because the autoconversion rate is proportional to  $q_c^{2.47}$ , the negatively skewed  $q_c$  also leads to a negatively skewed  $E_q$  in **Figure 7b**. As a result, the leg-averaged  $E_q$  diagnosed from the observation is slightly smaller than that derived based on Eq. **(6)** by assuming a lognormal distribution. The negative skewness also explains the large error in  $E_N$  for hleg 10 seen on **Figure 6b**. As shown in **Figure 7c** the observed  $N_c$  is also negatively skewed, to a much larger extent in comparison with  $q_c$ . Because the autoconversion rate is proportional to  $N_c^{-1.79}$ , the highly negatively skewed  $N_c$  results in a highly *positively* skewed  $E_N$  in **Figure 7d**. As a result, the  $E_N$  diagnosed from the observation is much larger than that derived based on Eq. **(7)** by assuming a lognormal distribution.

The  $E_q$  and  $E_N$  reflect only the individual contributions of subgrid  $q_c$  and  $N_c$  variations to the EF. The effect of the covariation of  $q_c$  and  $N_c$ , i.e., the  $E_{COV}$  is shown in **Figure 6c**. Interestingly, the value of  $E_{COV}$  is smaller than unity for all the selected hlegs. As explained in Eq. **(8)**,  $E_{COV} < 1$  is a result of a positive correlation between  $q_c$  and  $N_c$ , as seen in **Figure 4d**.

Deleted: Figure 4

Deleted: Figure 6

Deleted: (7)

Deleted: show a large error compared with

Formatted: Font: Not Italic

Deleted: ,

Deleted: hleg10

Deleted: Figure 7

Deleted: Figure 7

Formatted: Font color: Text 1

Formatted: Font: Not Italic, Font color: Text 1, Check spelling and grammar

Formatted: Font color: Text 1

Deleted: (6)

Deleted: Figure 6

Deleted: Figure 7

Deleted: Figure 7

Formatted: Font color: Text 1

Formatted: Font: Not Italic, Font color: Text 1, Check spelling and grammar

Formatted: Font color: Text 1

Deleted: (7)

Deleted: Figure 6

Formatted: Font: Not Italic

Deleted: (8)

Deleted: Figure 4

719 Therefore, in these hlegs the covariation of the  $q_c$  and  $N_c$  has *suppressing* effect on the EF, in  
 720 contrast to the enhancing effect of  $E_q$  and  $E_N$ . This result is qualitatively consistent with Z19 who  
 721 found that the vertically integrated liquid water path (LWP) of MBL clouds is in general positively  
 722 correlated with the  $N_c$  estimated from the MODIS cloud retrieval product and, as a result,  $E_{COV} <$   
 723 1 over most of the tropical oceans. Because of the relationship in Eq. (8), the value  $E_{COV}$  is  
 724 evidently negatively proportional to the correlation coefficient  $\rho_L$  in Figure 4d. The largest value  
 725 is seen in hleg 6 and 7 in which the bimodal joint distribution of  $q_c$  and  $N_c$  results in a small  $\rho_L$ . A  
 726 rather small value of  $E_{COV} \sim 0.45$  is seen for cloud top hleg 8 and 12, as result of a strong correlation  
 727 between  $q_c$  and  $N_c$  ( $\rho_L > 0.9$ ) and moderate  $\sigma_q$  and  $\sigma_N$ .

728 Finally, the EF that accounts for all factors, including the individual variations of  $q_c$  and  
 729  $N_c$ , as well as their covariation, is shown in Figure 6d. Focusing first on the observation-based  
 730 results (solid star), i.e.,  $E$  in Eq. (3), evidently there is a decreasing trend from cloud base (e.g.,  
 731  $E = 2.2$  for hleg 5 and  $E = 1.59$  for hleg 10) to cloud top (e.g.,  $E = 1.20$  for hleg 8 and  $E = 1.02$   
 732 for hleg 12). The  $E$  derived based on Eq. (5) by assuming the bi-variate lognormal distribution  
 733 between  $q_c$  and  $N_c$  (i.e., open star in Figure 6d) are in reasonable agreement with the observation-  
 734 based results, with a mean bias of  $-0.09$ . It is intriguing to note that the value of  $E = E_q \cdot E_N \cdot$   
 735  $E_{COV}$  in Figure 6d is comparable to  $E_q$  Figure 6a, which indicates that the enhancing effect of  $E_N >$   
 736 1 in Figure 6b is partially canceled by the suppressing effect of  $E_{COV} < 1$  in Figure 6c. As  
 737 aforementioned, many previous studies of the EF consider only the effect of  $E_q$  but overlook the  
 738 effect of  $E_N$  and  $E_{COV}$ . The error in the studies would be quite large if it were not for a fortunate  
 739 error cancellation.

## 740 5. Other Selected Cases

Deleted: (8)

Deleted: Figure 4

Deleted: The smallest

Deleted: =

Deleted: 21

Deleted: in

Deleted: =

Deleted: 96

Deleted: Figure 6

Deleted: (3)

Deleted: (5)

Deleted: Figure 6

Deleted: generally larger than the observation-based results, in particularly for hleg 6 and 7. To investigate the reason for this error, we compared the observed joint PDF between  $q_c$  and  $N_c$  for hleg 7 with the diagnosed bi-variate lognormal distribution in Figure 8. As already noted, the observed  $q_c$  and  $N_c$  follow a bimodal distribution which leads to a rather small correlation coefficient  $\rho_L$ . The bi-variate lognormal distribution interprets this small  $\rho_L$  as an abroad unimodal distribution (dashed contour line), which leads to an overestimate of EF. Finally, it

Deleted: Figure 6

Deleted: Figure 6

Deleted: Figure 6

Deleted: Figure 6

In addition to the July 18, 2017 RF, we also found another 6 RFs that meet our criteria as described in Section 3 for case selection, from non-precipitating (e.g., July 13, 2017 case in Figure S1), to weakly (e.g., Jan. 26, 2018 case in Figure S4) and heavily precipitating cloud (Feb. 11, 2018 case in Figure S6). Due to limited space, we cannot present the detailed case studies of these RFs. Instead, we view them collectively and investigate whether the lessons learned from the July 18, 2017 RF, especially those about the EF in Section 4.2, also apply to the other cases.

In order to compare the hlegs from different RFs, we first normalize the altitude of each hleg with respect to the minimum and maximum values of all selected hlegs in each RF as follows:

$$z_{hleg}^* = \frac{z_{hleg} - z_{min}}{z_{max} - z_{min}}, \quad (11)$$

where  $z_{hleg}^*$  is the normalized altitude for each hleg in a RF,  $z_{min}$  and  $z_{max}$  are the altitude of the lowest and highest hleg in the corresponding RF. Defined this way,  $z_{hleg}^*$  is bounded between 0 and 1. Alternatively,  $z_{hleg}^*$  could also be defined with respect to the averaged cloud top ( $z_{top}$ ) and base ( $z_{base}$ ) as inferred from the KAZR or vlegs. However, because of the variation of cloud top and cloud base heights, as well as the collocation error, the  $z_{hleg}^*$  would often become significantly larger than 1 or smaller than 0, if  $z_{hleg}^*$  were defined with respect to  $z_{top}$  and  $z_{base}$ , making results confusing and difficult to interpret.

Figure 8 shows the observation based EFs for all the selected hlegs from the 7 selected RFs as a function of the  $z_{hleg}^*$ . As shown in Figure 8a, the  $E$  derived based on Eq. (3) that accounts for the covariation of  $q_c$  and  $N_c$  has a decreasing trend from cloud base to cloud top. This is consistent with the result from the July 18, 2017 case in Figure 6d. However, neither the  $E_q$  in Figure 8b nor the  $E_N$  in Figure 8c shows a clear dependence on  $z_{hleg}^*$  in comparison with the results of July 18<sup>th</sup>,

Deleted: 3

Deleted: criteria

Deleted: . As summarized in Table 3 and shown in Figure 1c-h, the...

Deleted: 20

Deleted: and

Deleted: 19

Deleted: RFs sampled the MBL clouds around the ENA site repeatedly in a

Deleted: "V" shape horizontal pattern similar to the July 18, 2017 RF. In contrast, the

Deleted: .

Deleted: RF is different from the other three cases in two aspects. First, its horizontal sampling pattern is a simple straight line. Second, the boundary layer is significantly deeper, with a mean cloud top height around 1.5 km in comparison to the ~ 1 km cloud top height in other RFs.

Deleted: Figure 9

Deleted: 4

Deleted: Figure 9

Deleted: (3)

Deleted: Figure 6

Deleted: Figure 9

Deleted: Figure 9

2017 case in Figure 6a and b. Note that the  $E_q$  and  $E_N$  are influenced by a number of factors, such as horizontal distance and cloud fraction, in addition to vertical height. It is possible that the differences in other factors outweigh the vertical dependence here. Interestingly, the linear correlation coefficient  $\rho$  between  $q_c$  and  $N_c$  in Figure 8d shows an increasing trend with  $z_{hleg}^*$  that is statistically significant (R-value = 0.50 and P-value=0.02), despite a few outliers. This is consistent with what we found in the July 18, 2017 case (see Figure 4d). As evident from Eq. (8), an increase of  $\rho_L$  would lead to a decrease of  $E_{COV}$ . Since neither  $E_q$  nor  $E_N$  shows a clear dependence on  $z_{hleg}^*$ , the decrease of  $E_{COV}$  with  $z_{hleg}^*$  seems to play an important role in the determining the value of  $E$ . Another line of evidence supporting this role is the fact that both  $E_q$  and  $E_N$  are quite large for the cloud top hlegs, while in contrast the values of corresponding  $E$  that accounts for the covariation of  $q_c$  and  $N_c$  are much smaller. For example, the  $E_q$  for two hlegs from the Feb. 11, 2018 RF exceeds 8 but the corresponding  $E$  values are smaller than 1.2 which is evidently a result of large  $\rho_L$  and thereby small  $E_{COV}$ .

As aforementioned, many previous studies of the EF for the autoconversion rate parameterization consider only the effect of subgrid  $q_c$  variation but ignore the effects of subgrid  $N_c$  variation, and its covariation with  $q_c$ . To understand the potential error, we compared the  $E_q$  and  $E$  both derived based on observations in Figure 9. Apparently,  $E_q$  is significantly larger than  $E$  for most of the selected hlegs, which implies that the considering only subgrid  $q_c$  variation would likely lead to an overestimation of EF. This is an interesting result. Note that  $E_N \geq 1$  by definition and therefore  $E_q > E$  is possible only when the covariation of  $q_c$  and  $N_c$  has a suppressing effect, instead of enhancing. Once again, this result demonstrates the importance of understanding the covariation of  $q_c$  and  $N_c$  for understanding the EF for autoconversion rate parameterization.

Deleted: Figure 6

Deleted: Figure 9

Deleted: including the aforementioned hleg 6 and 7 from July 18, 2017 case and also the hleg 16 from Jan. 19, 2018 case. It turns out that the joint distribution of  $q_c$  and  $N_c$  in the hleg 16 of the Jan. 19, 2018 is also bimodal (similar to Figure 5b and not shown here), leading to a small  $\rho_L$ . Nevertheless, the increasing trend of  $\rho$  with  $z_{hleg}^*$  in Figure 9d...

Deleted: Figure 4

Deleted: (8)

Deleted: Figure 10

Deleted:  $E_q$

849 Having looked at the observation-based EFs, we now check if the EFs derived based on  
850 assumed PDFs (e.g., lognormal or bi-variate lognormal distributions) agree with the observation-  
851 based results. As shown in Figure 10a, the  $E_q$  based on Eq. (6), that assumes a lognormal  
852 distribution for the subgrid variation of  $q_c$  is in an excellent agreement with the observation-based  
853 results. In contrast, the comparison is much worse for the  $E_N$  in Figure 10b, which is not surprising  
854 given the results from the July 18, 2017 case in Figure 6b. As one can see from Figure 5, the  
855 marginal PDF of  $N_c$  is often broad and sometimes even bimodal. The deviation of the observed  
856  $N_c$  PDF from the lognormal distribution is probably the reason for the large difference of  $E_N$  in  
857 Figure 10b. As shown in Figure 10c, the  $E$  derived based on Eq. (5), by assuming a bi-variate  
858 lognormal function for the joint distribution of  $q_c$  and  $N_c$  are in good agreement with observation-  
859 based values, which is consistent with the results from the July 18, 2017 case in Figure 6.

## 860 6. Summary and Discussion

861 In this study we derived the horizontal variations of  $q_c$  and  $N_c$ , as well as their covariations in  
862 MBL clouds based on the in-situ measurements from the recent ACE-ENA campaign and  
863 investigated the implications of subgrid variability as relates to the enhancement of autoconversion  
864 rates. The main findings can be summarized as follows:

- 865 • In the July 18, 2017 case, the vertical variation of the mean values of  $q_c$  and  $N_c$  roughly  
866 follows the adiabatic structure. The horizontal variances of  $q_c$  and  $N_c$  first decrease from  
867 cloud base upward toward the middle of the cloud and then increase near cloud top. The  
868 correlation between of  $q_c$  and  $N_c$  generally increases from cloud base to cloud top.
- 869 • In other selected cases, the horizontal variances of  $q_c$  and  $N_c$  show no statistically  
870 significant dependence on the vertical height in cloud. However, the increasing trend of  
871 the correlation between  $q_c$  and  $N_c$  from cloud base to cloud top remains robust.

Deleted: Figure 11

Deleted: (6)

Deleted: Figure 11

Deleted: Figure 6

Deleted: Figure 5

Deleted: Figure 11

Deleted: Figure 11

Deleted: (5)

Deleted: and  $N_c$  tends to be larger than the observation-based results. The reason for this overestimation is because the joint PDF of  $q_c$  and  $N_c$  is often bimodal as seen in Figure 5. In such case, the small correlation coefficient  $\rho$  due to the bimodality is misinterpreted as a rather broad bi-variate lognormal distribution which in turn leads to an overestimated  $E$  value.

Formatted: Normal, TimesNewRoman, Indent: First line: 0"

Deleted: for

Deleted: EF

Deleted: the

Deleted: parameterization in the GCMs

Deleted: in the entrainment zone.

- In a few selected “V” shape hlegs, the  $q_c$  and  $N_c$  follow a bimodal joint distribution which leads to a weak linear correlation between them.
- The observation-based physically complete  $E$  that accounts for the covariation of  $q_c$  and  $N_c$  has a robust decreasing trend from cloud base to cloud top, which can be explained by the increasing trend of the  $q_c$  and  $N_c$  correlation from cloud base to cloud top.
- The  $E$  estimated by assuming a monomodal bi-variate lognormal joint distribution between  $q_c$  and  $N_c$  agrees well with the observation-based results.

**Deleted:** poor

**Deleted:** The two modes in the bimodal distribution correspond to the along-wind and cross-wind sides of the “V” shape hlegs.

**Deleted:** systematically overestimates the observation-based results, especially for the hlegs with a bimodal  $q_c$  and  $N_c$  joint distribution. The omission of the  $N_c$  variation and its covariation with  $q_c$  tends to lead to an overestimation of EF despite the error cancellation.

These results provide the following two new understandings of the EF for the autoconversion parameterization that have potentially important implications for GCM. First, our study indicates that the physically complete  $E$  has a robust decreasing trend from cloud base to cloud top. Because the autoconversion process is most important at the cloud top, this vertical dependence of EF should be taken into consideration in the GCM parametrization scheme. Second, our study indicates that effect of the  $q_c$  and  $N_c$  correlation plays a critical role in determining the EF. Lately a few novel modeling techniques have been developed to provide the coarse resolution GCMs information of subgrid cloud variation, such as the PDF-based higher-order turbulence closure method—Cloud Layer Unified By Binormals, CLUBB (Golaz et al., 2002; Guo et al., 2015; Larson et al., 2002). These models are able to provide parameterized subgrid variance of  $q_c$  which can be used in turn to estimate  $E_q$ . However, as shown in our study the  $E_q$  tends to overestimate the EF.

**Deleted:** (Golaz et al., 2002; Guo et al., 2015; Larson et al., 2002)...

Our study has a few of important limitations. First of all, our results are based on a handful cases from a single field campaign. The lessons learned here need to be further examined based on more data or tested in modeling studies. Second, as pointed out in section 4.1 due to the inherent sampling limitation of air-borne measurements, the temporal evolution of clouds is an important

**Deleted:** couple

**Deleted:** Second, we

928 uncertainty and a confounding factor in this study, which needs to be quantified in future studies.  
929 Third, our study provides only a phenomenological analysis of the horizontal variations cloud  
930 microphysics in the MBL clouds and the implications for the EF. Ongoing modeling research  
931 based on a comprehensive LES model is being conducted to identify and elucidate the process-  
932 level physical mechanisms behind our observational results. Finally, this study is focused on the  
933 KK parameterization in estimating the enhancement factors resulting from subgrid variability of  
934  $q_c$ ,  $N_c$  and  $q_c$ - $N_c$  covariance. The specific values are expected to differ when applied to other  
935 autoconversion parameterizations with different power-law exponents.  
936

937 **Acknowledgement:**

938 Z. Zhang acknowledges the financial support from the Atmospheric System Research (Grant DE-  
939 SC0020057) funded by the Office of Biological and Environmental Research in the US DOE Office of  
940 Science. The computations in this study were performed at the UMBC High Performance Computing  
941 Facility (HPCF). The facility is supported by the U.S. National Science Foundation through the MRI  
942 program (Grants CNS-0821258 and CNS-1228778) and the SCREMS program (Grant DMS-0821311),  
943 with substantial support from UMBC. Co-author D. Mechem was supported by subcontract OFED0010-  
944 01 from the University of Maryland Baltimore County and the U.S. Department of Energy's Atmospheric  
945 Systems Research grant DE-SC0016522.

946

947

948  
949  
950 Table 1 In situ cloud instruments from ACE-ENA campaign used in this study

Instruments	Measurements	Frequency	Resolution	Size resolution	Deleted: Accuracy
AIMMS	P, T, RH, u,v,w	20 Hz	/	/	
F-CDP	DSD 2~50 μm	10 Hz	1 -2 μm	2 μm	
2DS	DSD 10 ~2500 μm	1 Hz	25 – 150 μm	10 μm	

951  
952  
953 Table 2 conditions of MBL sampled during the two IOPs of ACE-ENA campaign

Conditions Sampled	Research Flights	
	IOP1: June-July 2017	IOP2: Jan.-Feb. 2018
Mostly clear	6/23, 6/29, 7/7	2/16
Thin Stratus	6/21, 6/25, 6/26, 6/28, 6/30, 7/4, 7/13	1/28, 2/1, 2/10, 2/12
Solid StCu	7/6, 7/8, 7/15	1/30, 2/7
Multi-layer StCu	7/11, 7/12	1/24, 1/29, 2/8
Drizzling StCu/Cu	7/3, 7/17, 7/18, 7/19, 7/20	1/19, 1/21, 1/25, 1/26, 2/9, 2/11, 2/15, 2/18, 2/19

954  
955 Table 3 A summary of selected RFs, and the selected hlegs and vlegs within each RF.

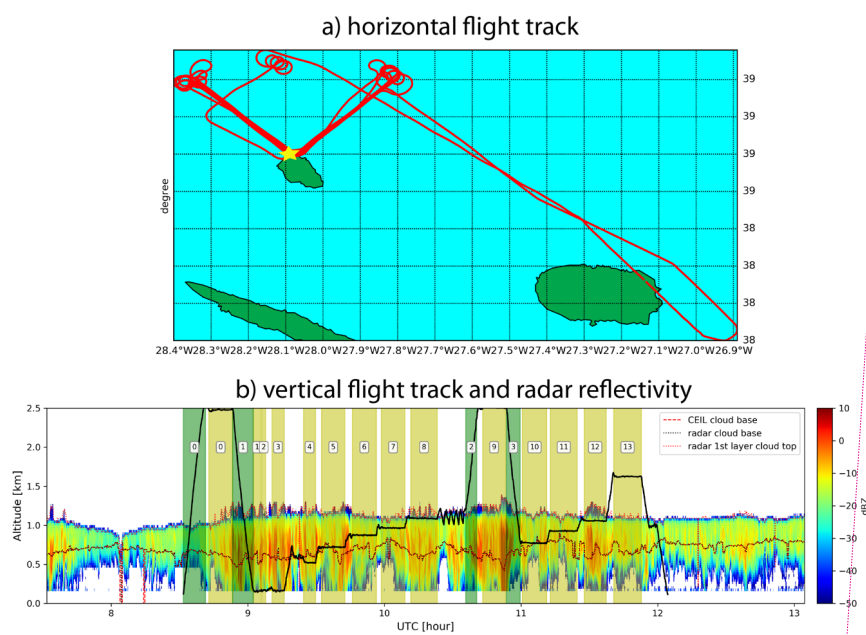
Research	Precipitation	Sampling	Selected hlegs	Selected	Inserted Cells
Flight		pattern		vlegs	
July 13, 2017	Non- Precipitating	Straight-line	3, 4, 5	0, 1, 3	
July 18, 2017	Precipitation	“V” shape	5, 6, 7, 8, 10, 11, 12	0, 1, 3	Deleted: IOP1
	reaching ground				Inserted Cells
July 20, 2017	Precipitation	“V” shape	5, 6, 7, 8, 9, 13, 14	0, 1	Formatted Table
	reaching ground				Deleted: IOP1
Jan. 19, 2018	Precipitation	“V” shape	6, 7, 8, 15, 16	0, 1, 3	Deleted: IOP2
	reaching ground				
Jan. 26, 2018	Precipitation only at	Straight-line	3, 4, 5, 9, 10, 11	0, 1, 3	
	cloud base				
Feb. 07, 2018	Non- Precipitating	“V” shape	1, 2, 3, 5	0, 1	

Feb. 11, 2018	Precipitation	Straight-line	4, 5, 6, 7, 12, 13	0, 1
	reaching ground			

- Formatted Table
- Deleted: IOP2
- Inserted Cells

960

961



964

965 Figure 1 (a) horizontal flight track of the G1 aircraft (red) during the July 18, 2017 RF, around the  
966 DOE ENA site (yellow star) on the Graciosa Island. The (b) vertical flight track of G1 (thick black  
967 line) overlaid on the radar reflectivity contour by the ground-based KZAR. The dotted lines in the  
968 figure indicate the cloud base and top retrievals from ground-based radar and CEIL instruments.  
969 The yellow shaded regions are the “hlegs” and green shaded regions are “vlegs”. See text for their  
970 definitions.

971

Deleted:

Deleted: Four selected RF from the ACE-ENA for this study. ...

Deleted: . Small arrows in

Deleted: figure indicate the wind vector at 900 mb.

Deleted: (c) and (d) same as (a) and (b), except for July 20, 2017 RF. (e) and (f) are for Jan. 19, 2018 RF. (g) and (h) are for Feb. 11, 2018 RF.

980

981

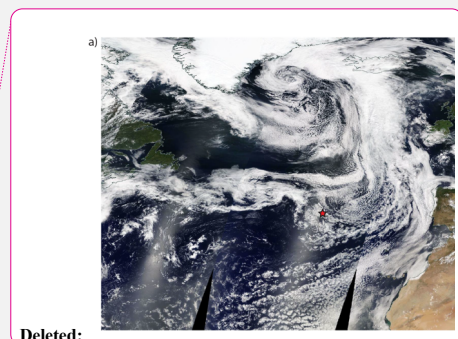
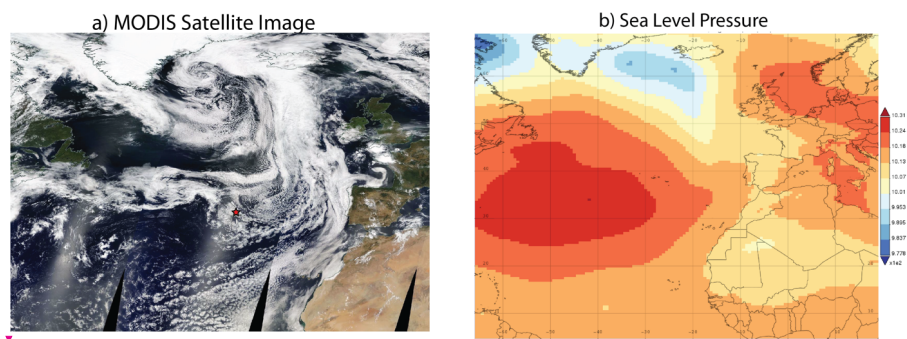
982

983

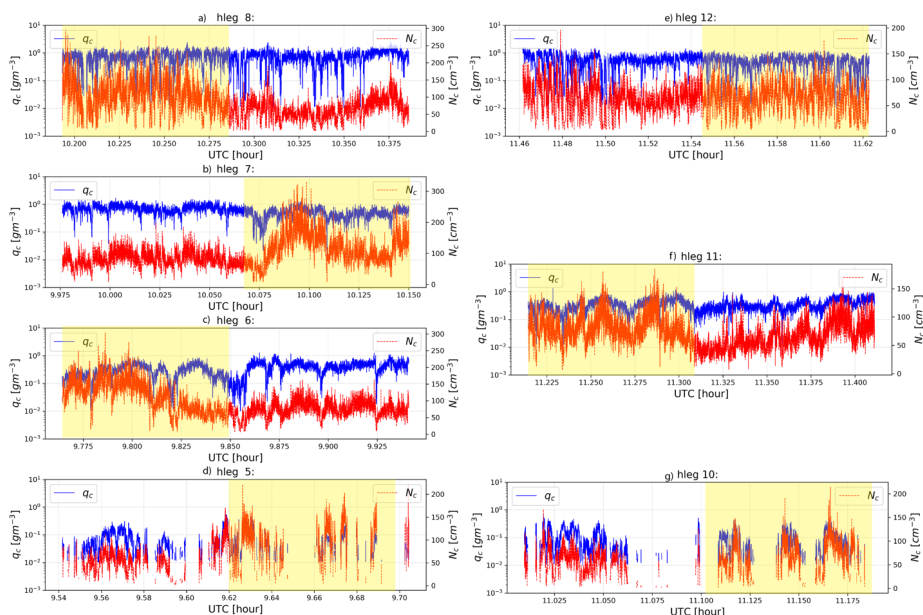
984

985

986



Deleted:



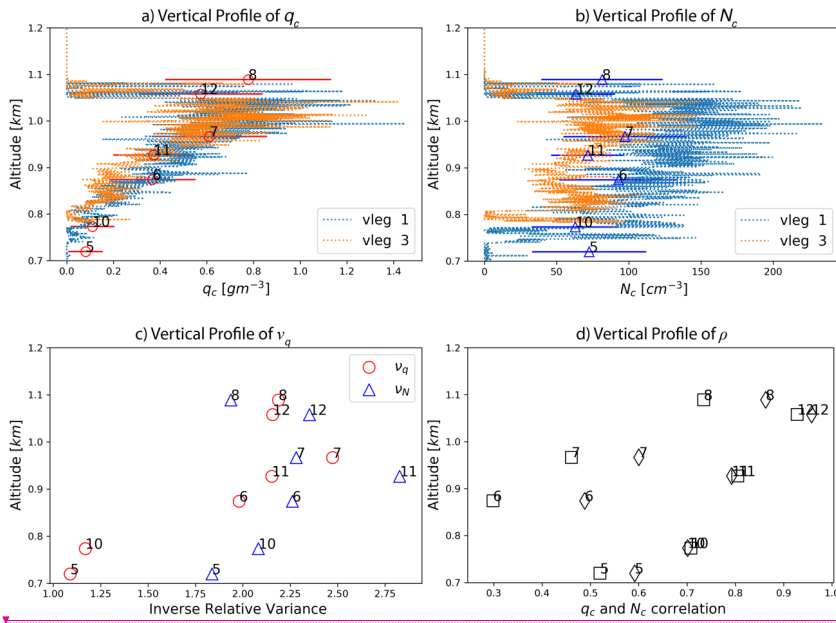
988

989 Figure 3 The horizontal variations of  $q_c$  (red) and  $N_c$  (blue) for each selected hleg derived from  
 990 the in situ FCDP instrument. The yellow-shaded time period in each plot corresponds to the  
 991 cross-wind side of the “V” shape flight track and the unshaded part corresponds to the along-  
 992 wind part. Note that plots are ordered such that the (a) hleg 8 and (e) hleg 12 are close to cloud  
 993 top; (b) hleg 6, (c) hleg 7 and (f) hleg 11 are sampled in the middle of clouds; (d) hleg 5 and (g)  
 994 hleg 10 are close to cloud base

995

Deleted:

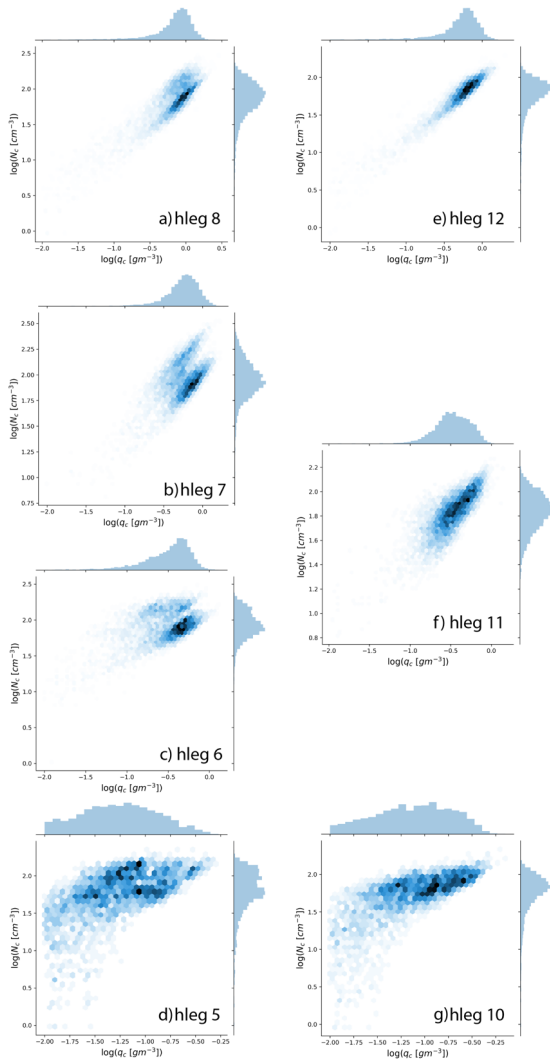
997  
998



999

Figure 4 (a) The vertical profiles of  $q_c$  derived from the vlegs (dotted lines) of the July 18, 2017 case. The overplotted red errorbars indicate the mean values and standard deviations of the  $q_c$  derived from the selected hlegs at different vertical levels. (b) same as (a) except for  $N_c$ . (c) The vertical profile of the inverse relative variances (i.e., mean divided by standard deviation) of  $N_c$  (red circle) and  $N_c$  (blue triangle) derived from the hleg; (d) The vertical profile of the linear correlation coefficient between  $\ln(q_c)$  and  $\ln(N_c)$ , i.e.,  $\rho_L$  (square) and linear correlation coefficient between  $q_c$  and  $N_c$ , i.e.,  $\rho$  (diamond).

1007



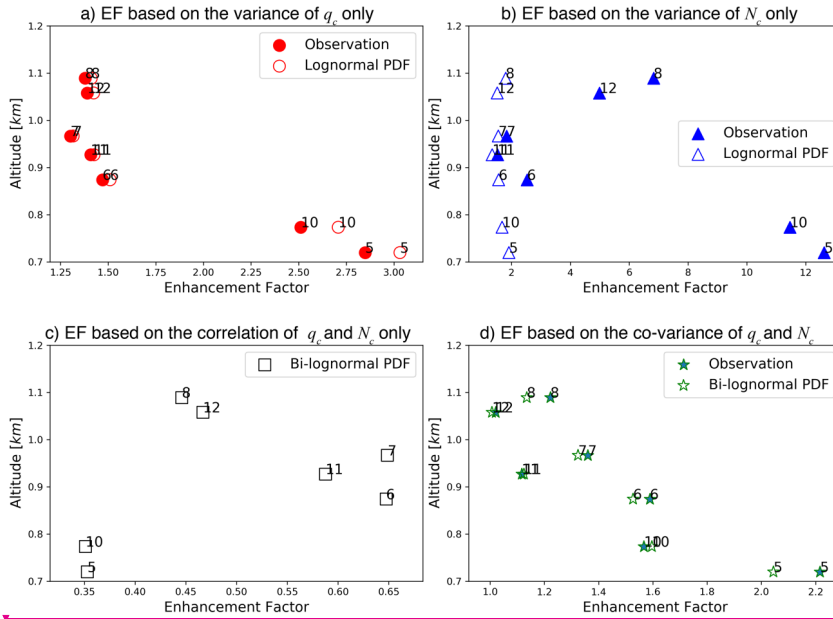
1009

1010 Figure 5 The joint distributions of the  $q_c$  and  $N_c$ , along with the marginal histograms, for the 7  
 1011 selected hleg from the July 18, 2017 RF. Same as Figure 3, the plots are ordered such that the (a)  
 1012 hleg 8 and (e) hleg 12 are close to cloud top; (b) hleg 6, (c) hleg 7 and (f) hleg 11 are sampled in  
 1013 the middle of clouds; (d) hleg 5 and (g) hleg 10 are close to cloud base.

1014

Deleted: Figure 3

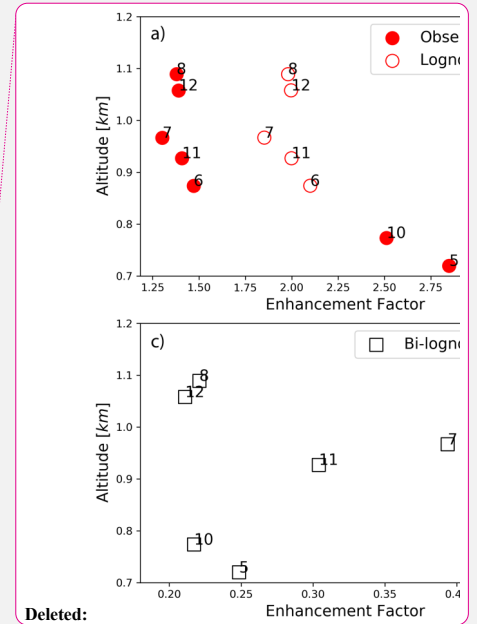
1016  
1017



1018

1019 Figure 6 (a)  $E_q$  as a function of height derived from observation based on Eq. (9) (solid circle)  
1020 and from the inverse relative variance  $v_q$  assuming lognormal distribution based on Eq. (6) (open  
1021 circle). (b)  $E_N$  as a function of height derived from observation based on Eq. (10) (solid triangle)  
1022 and from the inverse relative variance  $v_N$  assuming lognormal distribution based on Eq. (7)  
1023 (open triangle). (c)  $E_{COV}$  derived based on Eq. (8) as a function of height. (d)  $E$  as a function of  
1024 height derived from observation based on Eq. (3) (solid star) and based on Eq. (5) assuming a bi-  
1025 lognormal distribution (open star). The numbers beside the symbols in the figure correspond to  
1026 the numbers of the 7 selected hlegs.

1027



Deleted:

Formatted: Font: Not Italic

Deleted: (9)

Formatted: Font: Not Italic

Deleted: (6)

Formatted: Font: Not Italic

Deleted: (10)

Formatted: Font: Not Italic

Deleted: (7)

Formatted: Font: Not Italic

Deleted: (8)

Formatted: Font: Not Italic

Deleted: (3)

Formatted: Font: Not Italic

Deleted: (5)

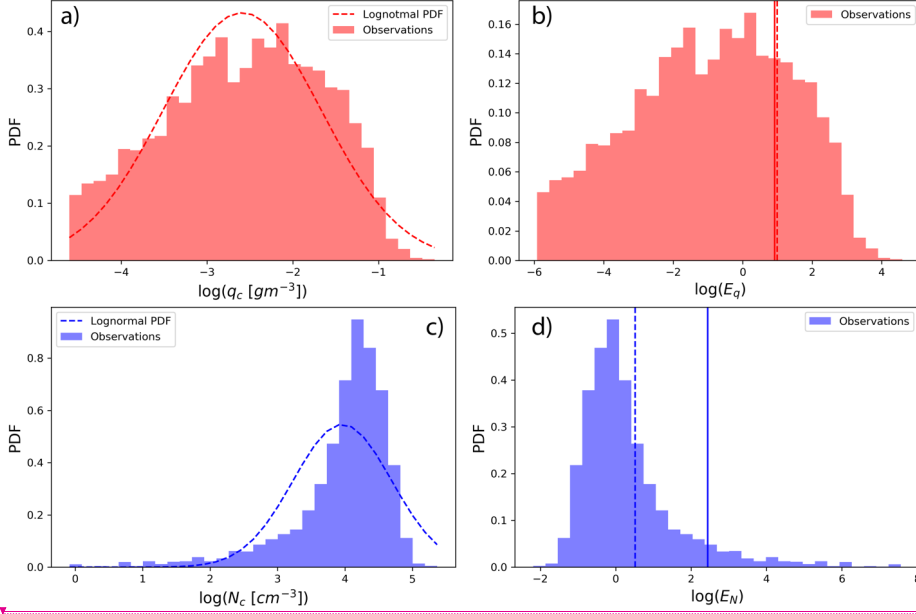
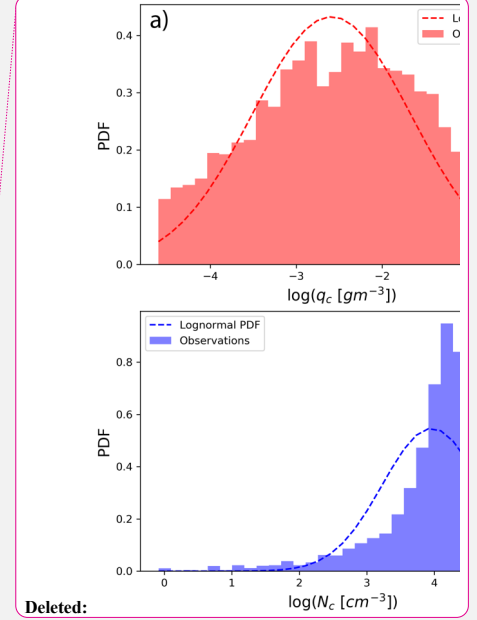


Figure 7 **(a)** Histogram of  $\ln(q_c)$  based on observations from the hleg 10 (bars) and the lognormal PDF (dashed line) based on the  $\mu_{q_c}$  and  $\sigma_{q_c}$  of hleg 10. **(b)** The histogram of  $\ln(E_q)$  diagnosed from the observed  $q_c$  based on Eq. (9). The two vertical lines correspond to the leg-averaged  $\ln(E_q)$  derived based on the observed  $q_c$  (solid) and the lognormal PDF (dashed line), respectively. **(c)** Histogram of  $\ln(N_c)$  based on observations from the hleg 10 (bars) and the lognormal PDF (dashed line) based on the  $\mu_{N_c}$  and  $\sigma_{N_c}$  of hleg 10. **(d)** The histogram of  $\ln(E_N)$  diagnosed from the observed  $q_c$  based on Eq. (10). The two vertical lines correspond to the leg-averaged  $\ln(E_N)$  derived based on the observed  $N_c$  (solid) and the lognormal PDF (dashed line), respectively.



Deleted:

Formatted: Font: Not Italic, Check spelling and grammar

Deleted: (9)

Formatted: Do not check spelling or grammar

Formatted: Font: Not Italic

Formatted: Do not check spelling or grammar

Deleted: (10)

1052



1059

.....Page Break.....

.. [1]

**Deleted:** (11)

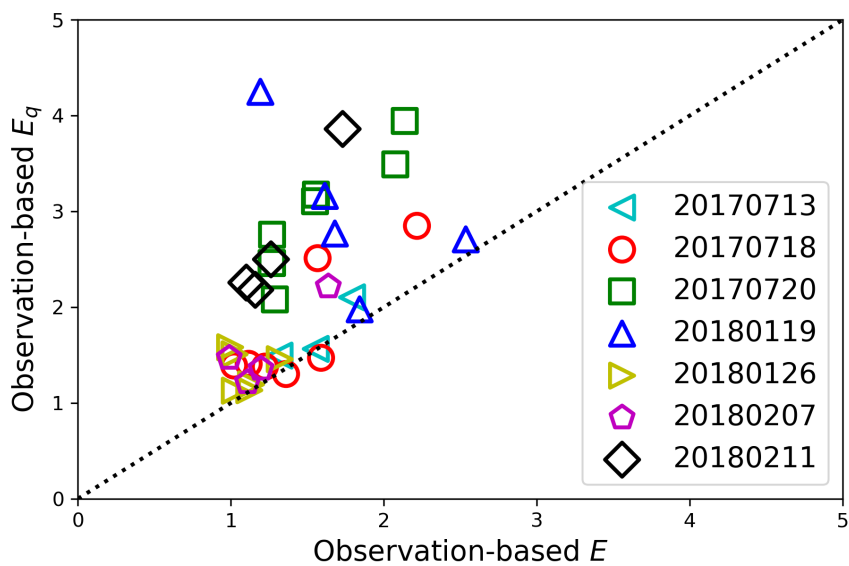
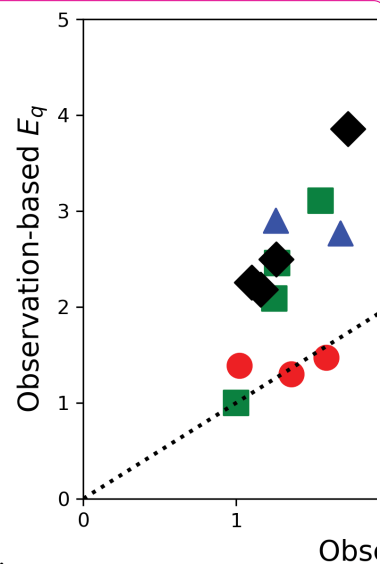


Figure 9 A comparison of observation-based  $E$  and observation-based  $E_q$  for all the selected hlegs from all 4 selected RF.



Deleted:

Deleted: 10

1096

1097

1098

1099

1100

1101

1102

1103

1104

1105

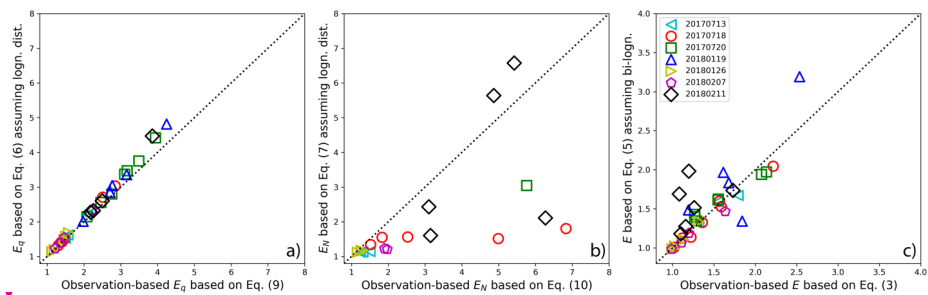
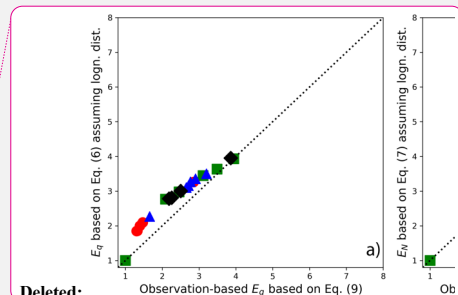


Figure 10. (a) A comparison of observation-based  $E_q$  derived based on Eq. (9) and  $E_q$  derived based on Eq. (6) assuming lognormal distribution for subgrid  $q_c$  observations for all the selected hlegs. (b) A comparison of observation-based  $E_N$  derived based on Eq. (10) and  $E_N$  derived based on Eq. (7) assuming lognormal distribution for all the selected hlegs. (c) A comparison of observation-based  $E$  derived based on Eq. (3) and  $E$  derived based on Eq. (5) assuming bi-variate lognormal distribution for the subgrid joint distribution of  $q_c$  and  $N_c$ .



- Deleted:
- Deleted: 11
  - Formatted: Font: Italic
  - Deleted: (9)
  - Formatted: Font: Italic
  - Deleted: (6)
  - Formatted: Font: Italic
  - Formatted: Font: Italic
  - Deleted: 12
  - Formatted: Font: Italic
  - Formatted: Font: Italic
  - Deleted: (10)
  - Formatted: Font: Italic
  - Formatted: Font: Italic
  - Deleted: (7)
  - Deleted: (3)
  - Deleted: (5)

1115

1116 **References:**

- 1117 Ahlgrim, M. and Forbes, R. M.: Regime dependence of cloud condensate variability observed  
1118 at the Atmospheric Radiation Measurement Sites, Quarterly Journal of the Royal Meteorological  
1119 Society, 142(697), 1605–1617, doi:10.1002/qj.2783, 2016.
- 1120 Barker, H. W., Wielicki, B. A. and Parker, L.: A Parameterization for Computing Grid-  
1121 Averaged Solar Fluxes for Inhomogeneous Marine Boundary Layer Clouds. Part II: Validation  
1122 Using Satellite Data, [http://dx.doi.org/10.1175/1520-0469\(1996\)053<2304:APFCGA>2.0.CO;2](http://dx.doi.org/10.1175/1520-0469(1996)053<2304:APFCGA>2.0.CO;2),  
1123 53(16), 2304–2316 [online] Available from: <http://journals.ametsoc.org/doi/pdf/10.1175/1520-0469%281996%29053%3C2304%3AAPFCGA%3E2.0.CO%3B2>, 1996.
- 1125 Beswick, K. M., Gallagher, M. W., Webb, A. R., Norton, E. G. and Perry, F.: Application of the  
1126 Aventech AIMMS20AQ airborne probe for turbulence measurements during the Convective  
1127 Storm Initiation Project, Atmospheric Chemistry and Physics, 8(17), 5449–5463,  
1128 doi:10.5194/acp-8-5449-2008, 2008.
- 1129 Bony, S. and Dufresne, J.-L.: Marine boundary layer clouds at the heart of tropical cloud  
1130 feedback uncertainties in climate models, Geophysical Research Letters, 32(20), L20806,  
1131 doi:10.1029/2005GL023851, 2005.
- 1132 Bony, S., Stevens, B., Frierson, D. M. W., Jakob, C., Kageyama, M., Pincus, R., Shepherd, T. G.,  
1133 Sherwood, S. C., Siebesma, A. P., Sobel, A. H., Watanabe, M. and Webb, M. J.: Clouds,  
1134 circulation and climate sensitivity, Nature Geoscience, 8(4), 261–268, doi:10.1038/ngeo2398,  
1135 2015.
- 1136 Boucher, O., Randall, D., Artaxo, P., Bretherton, C., Feingold, G., Forster, P., Kerminen, V.-M.,  
1137 Kondo, Y., Liao, H. and Lohmann, U.: Clouds and aerosols, in Climate change 2013: The  
1138 physical science basis. Contribution of working group I to the fifth assessment report of the  
1139 intergovernmental panel on climate change, pp. 571–657, Cambridge University Press. 2013.
- 1140 Boutle, I. A., Abel, S. J., Hill, P. G. and Morcrette, C. J.: Spatial variability of liquid cloud and  
1141 rain: observations and microphysical effects, Quarterly Journal of the Royal Meteorological  
1142 Society, 140(679), 583–594, doi:10.1002/qj.2140, 2014.
- 1143 Brenguier, J., Pawlowska, H. and Schüller, L.: Radiative properties of boundary layer clouds:  
1144 Droplet effective radius versus number ....., 2000.
- 1145 Cahalan, R. F. and Joseph, J. H.: Fractal statistics of cloud fields, Monthly Weather Review,  
1146 117(2), 261–272, 1989.
- 1147 Carslaw, K. S., Lee, L. A., Reddington, C. L., Pringle, K. J., Rap, A., Forster, P. M., Mann, G.  
1148 W., Spracklen, D. V., Woodhouse, M. T., Regayre, L. A. and Pierce, J. R.: Large contribution of  
1149 natural aerosols to uncertainty in indirect forcing, Nature, 503(7474), 67–71,  
1150 doi:10.1038/nature12674, 2013.

Formatted: Font: Not Italic

1151 Clothiaux, E. E., Marchand, R. T., Martner, B. E., Ackerman, T. P., Mace, G. G., Moran, K. P.,  
 1152 Miller, M. A. and Martner, B. E.: Objective Determination of Cloud Heights and Radar  
 1153 Reflectivities Using a Combination of Active Remote Sensors at the ARM CART Sites,  
 1154 [http://dx.doi.org/10.1175/1520-0450\(2000\)039<0645:ODOCHA>2.0.CO;2](http://dx.doi.org/10.1175/1520-0450(2000)039<0645:ODOCHA>2.0.CO;2), 39(5), 645–665,  
 1155 doi:10.1175/1520-0450(2000)039<0645:ODOCHA>2.0.CO;2, 2000.

1156 Dong, X., Xi, B., Kennedy, A., Minnis, P. and Wood, R.: A 19-Month Record of Marine  
 1157 Aerosol–Cloud–Radiation Properties Derived from DOE ARM Mobile Facility Deployment at  
 1158 the Azores. Part I: Cloud Fraction and Single-Layered MBL Cloud Properties,  
 1159 <http://dx.doi.org/10.1175/JCLI-D-13-00553.1>, 27(10), 3665–3682, doi:10.1175/JCLI-D-13-  
 1160 00553.1, 2014.

1161 Golaz, J.-C., Larson, V. E. and Cotton, W. R.: A PDF-Based Model for Boundary Layer Clouds.  
 1162 Part I: Method and Model Description, *JAS*, 59(24), 3540–3551, doi:10.1175/1520-  
 1163 0469(2002)059<3540:APBMFB>2.0.CO;2, 2002.

1164 Grosvenor, D. P., Sourdeval, O., Zuidema, P., Ackerman, A., Alexandrov, M. D., Bennartz, R.,  
 1165 Boers, R., Cairns, B., Chiu, J. C., Christensen, M., Deneke, H., Diamond, M., Feingold, G.,  
 1166 Fridlind, A., Hunerbein, A., Knist, C., Kollias, P., Marshak, A., McCoy, D., Merk, D., Painemal,  
 1167 D., Rausch, J., Rosenfeld, D., Russchenberg, H., Seifert, P., Sinclair, K., Stier, P., van  
 1168 Diedenhoven, B., Wendisch, M., Werner, F., Wood, R., Zhang, Z. and Quaas, J.: Remote  
 1169 Sensing of Droplet Number Concentration in Warm Clouds: A Review of the Current State of  
 1170 Knowledge and Perspectives, *Reviews of Geophysics*, 56(2), 409–453,  
 1171 doi:10.1029/2017RG000593, 2018.

1172 Guo, H., Golaz, J. C., Donner, L. J., Wyman, B., Zhao, M. and Ginoux, P.: CLUBB as a unified  
 1173 cloud parameterization: Opportunities and challenges, *Geophysical Research Letters*, 42(11),  
 1174 4540–4547, doi:10.1002/2015GL063672, 2015.

1175 Hill, P. G., Morcrette, C. J. and Boutle, I. A.: A regime-dependent parametrization of subgrid-  
 1176 scale cloud water content variability, *Quarterly Journal of the Royal Meteorological Society*,  
 1177 141(691), 1975–1986, doi:10.1002/qj.2506, 2015.

1178 Huang, D. and Liu, Y.: Statistical characteristics of cloud variability. Part 2: Implication for  
 1179 parameterizations of microphysical and radiative transfer processes in climate models, *Journal of*  
 1180 *Geophysical Research-Atmospheres*, 119(18), 10,829–10,843, doi:10.1002/2014JD022003,  
 1181 2014.

1182 Huang, D., Campos, E. and Liu, Y.: Statistical characteristics of cloud variability. Part 1:  
 1183 Retrieved cloud liquid water path at three ARM sites, *Journal of Geophysical Research-*  
 1184 *Atmospheres*, 119(18), 10,813–10,828, doi:10.1002/2014JD022001, 2014.

1185 Khairoutdinov, M. and Kogan, Y.: A New Cloud Physics Parameterization in a Large-Eddy  
 1186 Simulation Model of Marine Stratocumulus, *Mon. Wea. Rev.*, 128(1), 229–243 [online]  
 1187 Available from: [http://journals.ametsoc.org/doi/abs/10.1175/1520-](http://journals.ametsoc.org/doi/abs/10.1175/1520-0493(2000)128%3C0229%3AANCPPI%3E2.0.CO%3B2)  
 1188 [0493\(2000\)128%3C0229%3AANCPPI%3E2.0.CO%3B2](http://journals.ametsoc.org/doi/abs/10.1175/1520-0493(2000)128%3C0229%3AANCPPI%3E2.0.CO%3B2), 2000.

1189 Kogan, Y. L. and Mechem, D. B.: A PDF-Based Microphysics Parameterization for Shallow  
 1190 Cumulus Clouds, *J. Atmos. Sci.*, 71(3), 1070–1089, doi:10.1175/JAS-D-13-0193.1, 2014.

1191 Kogan, Y. L. and Mechem, D. B.: A PDF-Based Formulation of Microphysical Variability in  
 1192 Cumulus Congestus Clouds, *J. Atmos. Sci.*, 73(1), 167–184, doi:10.1175/JAS-D-15-0129.1,  
 1193 2016.

1194 Kollias, P., ALBRECHT, B. A., Clothiaux, E. E., Miller, M. A., Johnson, K. L. and Moran, K.  
 1195 P.: The Atmospheric Radiation Measurement Program Cloud Profiling Radars: An Evaluation of  
 1196 Signal Processing and Sampling Strategies, <http://dx.doi.org/10.1175/JTECH1749.1>, 22(7), 930–  
 1197 948, doi:10.1175/JTECH1749.1, 2005.

1198 Lance, S., Brock, C. A., Rogers, D. and Gordon, J. A.: Water droplet calibration of the Cloud  
 1199 Droplet Probe (CDP) and in-flight performance in liquid, ice and mixed-phase clouds during  
 1200 ARCPAC, *AMT*, 3(6), 1683–1706, doi:10.5194/amt-3-1683-2010, 2010.

1201 Larson, V. E. and Griffin, B. M.: Analytic upscaling of a local microphysics scheme. Part I:  
 1202 Derivation, *Quarterly Journal of the Royal Meteorological Society*, 139(670), 46–57,  
 1203 doi:10.1002/qj.1967, 2013.

1204 Larson, V. E., Golaz, J.-C. and Cotton, W. R.: Small-Scale and Mesoscale Variability in Cloudy  
 1205 Boundary Layers: Joint Probability Density Functions, *J. Atmos. Sci.*, 59(24), 3519–3539,  
 1206 doi:10.1175/1520-0469(2002)059<3519:SSAMVI>2.0.CO;2, 2002.

1207 Lebsock, M., Morrison, H. and Gettelman, A.: Microphysical implications of cloud-precipitation  
 1208 covariance derived from satellite remote sensing, *Journal of Geophysical Research-Atmospheres*,  
 1209 118(12), 6521–6533, doi:10.1002/jgrd.50347, 2013.

1210 Liu, Y. and Daum, P. H.: Parameterization of the Autoconversion Process. Part I: Analytical  
 1211 Formulation of the Kessler-Type Parameterizations, [http://dx.doi.org/10.1175/1520-](http://dx.doi.org/10.1175/1520-0469(2004)061<1539:POTAPI>2.0.CO;2)  
 1212 [0469\(2004\)061<1539:POTAPI>2.0.CO;2](http://dx.doi.org/10.1175/1520-0469(2004)061<1539:POTAPI>2.0.CO;2), 61(13), 1539–1548, doi:10.1175/1520-  
 1213 [0469\(2004\)061<1539:POTAPI>2.0.CO;2](http://dx.doi.org/10.1175/1520-0469(2004)061<1539:POTAPI>2.0.CO;2), 2004.

1214 Lohmann, U. and Feichter, J.: Global indirect aerosol effects: a review, *ACP*, 5(3), 715–737,  
 1215 2005.

1216 Martin, G., Johnson, D. and Spice, A.: The Measurement and Parameterization of Effective  
 1217 Radius of Droplets in Warm Stratocumulus Clouds, 51(13), 1823–1842, 1994.

1218 **Matthews, A. and Mei, F.: WCM water content for ACE-ENA, n.d.**

1219 Morrison, H. and Gettelman, A.: A New Two-Moment Bulk Stratiform Cloud Microphysics  
 1220 Scheme in the Community Atmosphere Model, Version 3 (CAM3). Part I: Description and  
 1221 Numerical Tests, *Journal of Climate*, 21(15), 3642–3659, doi:10.1175/2008JCLI2105.1, 2008.

1222 Pincus, R. and Klein, S. A.: Unresolved spatial variability and microphysical process rates in  
 1223 large-scale models, *J. Geophys. Res.*, 105(D22), 27059–27065, doi:10.1029/2000JD900504,  
 1224 2000.

Moved (insertion) [1]

Formatted: Font: Not Italic

1225 Rémillard, J., Kollias, P., Luke, E. and Wood, R.: Marine Boundary Layer Cloud Observations in  
1226 the Azores, *Journal of Climate*, 25(21), 7381–7398, doi:10.1175/JCLI-D-11-00610.1, 2012.

1227 SPEC: SPEC FCDP Technical Manual (Rev.2.0). 2019.

1228 Voyles, J. W. and Mather, J. H.: The Arm Climate Research Facility: A Review of Structure and  
1229 Capabilities, American Meteorological Society. 2013.

1230 [Walters, D., Baran, A. J., Boutle, I., Brooks, M., Earnshaw, P., Edwards, J., Furtado, K., Hill, P.,](#)  
1231 [Lock, A., Manners, J., Morcrette, C., Mulcahy, J., Sanchez, C., Smith, C., Stratton, R., Tennant,](#)  
1232 [W., Tomassini, L., Van Weverberg, K., Vosper, S., Willett, M., Browse, J., Bushell, A., Carslaw,](#)  
1233 [K., Dalvi, M., Essery, R., Gedney, N., Hardiman, S., Johnson, B., Johnson, C., Jones, A., Jones,](#)  
1234 [C., Mann, G., Milton, S., Rumbold, H., Sellar, A., Ujiie, M., Whittall, M., Williams, K. and](#)  
1235 [Zerroukat, M.: The Met Office Unified Model Global Atmosphere 7.0/7.1 and JULES Global](#)  
1236 [Land 7.0 configurations, \*Geosci. Model Dev.\*, 12\(5\), 1909–1963, doi:10.5194/gmd-12-1909-](#)  
1237 [2019, 2019.](#)

1238 Wang, J., Dong, X. and Wood, R.: Aerosol and Cloud Experiments in Eastern North Atlantic  
1239 (ACE-ENA) Science Plan, DOE Office of Science Atmospheric Radiation Measurement (ARM)  
1240 Program .... 2016.

1241 Wood, R.: Drizzle in Stratiform Boundary Layer Clouds. Part I: Vertical and Horizontal  
1242 Structure, *J. Atmos. Sci.*, 62(9), 3011–3033, doi:10.1175/JAS3529.1, 2005a.

1243 Wood, R.: Drizzle in stratiform boundary layer clouds. Part II: Microphysical aspects,, 62(9),  
1244 3034–3050, 2005b.

1245 Wood, R.: Stratocumulus Clouds, *Mon. Wea. Rev.*, 140(8), 2373–2423, doi:10.1175/MWR-D-  
1246 11-00121.1, 2012.

1247 Wood, R. and Hartmann, D. L.: Spatial Variability of Liquid Water Path in Marine Low Cloud:  
1248 The Importance of Mesoscale Cellular Convection, *J. Climate*, 19(9), 1748–1764,  
1249 doi:10.1175/JCLI3702.1, 2006.

1250 Wood, R., Wyant, M., Bretherton, C. S., Rémillard, J., Kollias, P., Fletcher, J., Stemmler, J., de  
1251 Szoce, S., Yuter, S., Miller, M., Mechem, D., Tselioudis, G., Chiu, J. C., Mann, J. A. L.,  
1252 O'Connor, E. J., Hogan, R. J., Dong, X., Miller, M., Ghate, V., Jefferson, A., Min, Q., Minnis, P.,  
1253 Palikonda, R., Albrecht, B., Luke, E., Hannay, C. and Lin, Y.: Clouds, Aerosols, and  
1254 Precipitation in the Marine Boundary Layer: An Arm Mobile Facility Deployment, *Bulletin of*  
1255 *the American Meteorological Society*, 96(3), 419–440, doi:10.1175/BAMS-D-13-00180.1, 2015.

1256 Wu, P., Xi, B., Dong, X. and Zhang, Z.: Evaluation of autoconversion and accretion  
1257 enhancement factors in general circulation model warm-rain parameterizations using ground-  
1258 based measurements over the Azores, *Atmospheric Chemistry and Physics*, 18(23), 17405–  
1259 17420, doi:10.5194/acp-18-17405-2018, 2018.

Formatted: Font: Not Italic

1260 Xie, X. and Zhang, M.: Scale-aware parameterization of liquid cloud inhomogeneity and its  
 1261 impact on simulated climate in CESM, *Journal of Geophysical Research-Atmospheres*, 120(16),  
 1262 8359–8371, doi:10.1002/2015JD023565, 2015.

1263 Zhang, Z. and Platnick, S.: An assessment of differences between cloud effective particle radius  
 1264 retrievals for marine water clouds from three MODIS spectral bands, *J Geophys Res*, 116(D20),  
 1265 D20215, doi:10.1029/2011JD016216, 2011.

1266 Zhang, Z., Ackerman, A. S., Feingold, G., Platnick, S., Pincus, R. and Xue, H.: Effects of cloud  
 1267 horizontal inhomogeneity and drizzle on remote sensing of cloud droplet effective radius: Case  
 1268 studies based on large-eddy simulations, *J Geophys Res*, 117(D19), D19208–,  
 1269 doi:10.1029/2012JD017655, 2012.

1270 Zhang, Z., Dong, X., Xi, B., Song, H., Ma, P.-L., Ghan, S. J., Platnick, S. and Minnis, P.:  
 1271 Intercomparisons of marine boundary layer cloud properties from the ARM CAP-MBL  
 1272 campaign and two MODIS cloud products, *Journal of Geophysical Research-Atmospheres*,  
 1273 122(4), 2351–2365, doi:10.1002/2016JD025763, 2017.

1274 Zhang, Z., Song, H., Ma, P.-L., Larson, V. E., Wang, M., Dong, X. and Wang, J.: Subgrid  
 1275 variations of the cloud water and droplet number concentration over the tropical ocean: satellite  
 1276 observations and implications for warm rain simulations in climate models, *Atmospheric*  
 1277 *Chemistry and Physics*, 19(2), 1077–1096, doi:10.5194/acp-19-1077-2019, 2019.

1278 Zhang, Z., Werner, F., Cho, H. M., Wind, G., Platnick, S., Ackerman, A. S., Di Girolamo, L.,  
 1279 Marshak, A. and Meyer, K.: A framework based on 2-D Taylor expansion for quantifying the  
 1280 impacts of sub-pixel reflectance variance and covariance on cloud optical thickness and effective  
 1281 radius retrievals based on the bi-spectral method, *Journal of Geophysical Research-Atmospheres*,  
 1282 2016JD024837, doi:10.1002/2016JD024837, 2016.

1283 Zheng, X., Klein, S. A., Ma, H. Y., Bogenschütz, P., Gettelman, A. and Larson, V. E.:  
 1284 Assessment of marine boundary layer cloud simulations in the CAM with CLUBB and updated  
 1285 microphysics scheme based on ARM observations from the Azores, *Journal of Geophysical*  
 1286 *Research-Atmospheres*, doi:10.1002/2016JD025274, 2016.

Moved up [1]: n.d.¶

**Deleted:** *Improving and Understanding Climate Models: Scale-Aware Parameterization of Cloud Water Inhomogeneity and Sensitivity of MJO Simulation to Physical Parameters in a Convection Scheme - ProQuest, search.proquest.com [online]. Available from: <https://search.proquest.com/docview/1964630004?pq-origsite=gscholar> (Accessed 5 February 2018).*

**Deleted:** Xie, X. and Zhang, M.:

**Formatted:** Font: Not Italic

**Formatted:** Font: Not Italic

**Formatted:** Font: 12 pt, Not Italic

